Fast Ewald Summation based on NFFT with Mixed Periodicity

Franziska Nestler, Michael Pippig and Daniel Potts

In this paper we develop new fast Fourier-based methods for the Coulomb problem. We combine the Ewald summation formulas and the fast summation approach based on the nonequispaced fast Fourier transform (NFFT) in order to develop efficient methods for calculating the Coulomb potentials as well as the acting forces in charged particle systems subject to mixed periodic boundary conditions. Therewith, we extend the applicability of NFFT based methods, which already exist for open as well as for 3d-periodic boundary conditions, to arbitrary combinations of periodic and open boundary conditions. We reconsider the derivation of the Ewald formulas for 2d- and 1d-periodic systems, introduce the new algorithms and present numerical results.

Key words and phrases : Ewald method, nonequispaced fast Fourier transform, particle methods, NFFT, FMM, P3M, P2NFFT

2000 AMS Mathematics Subject Classification : 65T

1. Introduction

Let N charges $q_j \in \mathbb{R}$ at positions $\boldsymbol{x}_j \in \mathbb{R}^3$, $j = 1, \ldots, N$, be given, fulfilling the charge neutrality condition

$$\sum_{j=1}^{N} q_j = 0\,. \tag{1.1}$$

The Coulomb energy is basically a sum of the form

$$U_{\mathcal{S}} := \frac{1}{2} \sum_{j=1}^{N} q_j \phi_{\mathcal{S}}(\boldsymbol{x}_j), \tag{1.2}$$

franziska.nestler@mathematik.tu-chemnitz.de,
michael.pippig@mathematik.tu-chemnitz.de,
potts@mathematik.tu-chemnitz.de,
Technische Universität Chemnitz, Faculty of Mathematics, 09107 Chemnitz, Germany

where for each particle j the potential $\phi_{\mathcal{S}}(\boldsymbol{x}_j)$ is given by

$$\phi_{\mathcal{S}}(\boldsymbol{x}_j) := \sum_{\boldsymbol{n}\in\mathcal{S}} \sum_{i=1}^{N}{}' \frac{q_i}{\|\boldsymbol{x}_{ij} + B\boldsymbol{n}\|}. \tag{1.3}$$

Thereby, we denote by $\|\cdot\|$ the Euclidean norm and define the difference vectors $\boldsymbol{x}_{ij} := \boldsymbol{x}_i - \boldsymbol{x}_j$. The set of translation vectors $\mathcal{S} \subseteq \mathbb{Z}^3$ is defined according to the given boundary conditions and $B \in \mathbb{R}$ is the edge length of the simulation box in each dimension subject to periodic boundary conditions. The prime on the double sum indicates that for $\boldsymbol{n} = \boldsymbol{0}$ all terms with $i = j$ are omitted. It is important to note that the sum (1.3) is, assuming charge neutrality (1.1), only conditionally convergent, i.e., the values of the potentials $\phi_{\mathcal{S}}(\boldsymbol{x}_j)$ depend on the order of summation. In addition to the calculation of the potentials $\phi_{\mathcal{S}}(\boldsymbol{x}_j)$ and the total energy $U_{\mathcal{S}}$ of the system, we are also interested in evaluating the forces acting on the particles, which are given by

$$\boldsymbol{F}_{\mathcal{S}}(\boldsymbol{x}_j) := q_j \boldsymbol{E}_{\mathcal{S}}(\boldsymbol{x}_j), \quad \text{with the fields} \quad \boldsymbol{E}_{\mathcal{S}}(\boldsymbol{x}_j) := -\nabla\phi_{\mathcal{S}}(\boldsymbol{x}_j). \tag{1.4}$$

The well known Ewald-Summation technique [16], which was originally developed for 3d-periodic systems, where we set $\mathcal{S} := \mathbb{Z}^3$ in our notation, is the main basis for a variety of fast algorithms for the evaluation of (1.2) under fully periodic boundary conditions, see [26, 13, 12, 15, 20]. The Ewald summation method [16] makes use of the trivial identity

$$\frac{1}{r} = \frac{\operatorname{erf}(\alpha r)}{r} + \frac{\operatorname{erfc}(\alpha r)}{r}, \tag{1.5}$$

where $\alpha > 0$ is generally known as the splitting parameter, $\operatorname{erf}(x) := \frac{2}{\sqrt{\pi}} \int_0^x \mathrm{e}^{-t^2} \mathrm{d}t$ is the well known error function and $\operatorname{erfc}(x) := 1 - \operatorname{erf}(x)$ is the complementary error function. If (1.5) is applied in (1.3) the potential $\phi_{\mathcal{S}}(\boldsymbol{x}_j)$ is split into two rapidly converging parts. Thereby, the erf-terms have the finite limit

$$\lim_{r\to 0} \frac{\operatorname{erf}(\alpha r)}{r} = \frac{2\alpha}{\sqrt{\pi}}, \tag{1.6}$$

so that this part can be transformed into a sum in Fourier space, which allows the application of fast Fourier methods in order to derive efficient algorithms. The second part, containing the complementary error function, is absolutely convergent and can be calculated by a direct summation after truncating the infinite sum.

We describe 2d-periodic boundary conditions by choosing $\mathcal{S} := \mathbb{Z}^2 \times \{0\}$ with $\boldsymbol{x}_j \in B\mathbb{T}^2 \times \mathbb{R}$ and 1d-periodic constraints by choosing $\mathcal{S} := \mathbb{Z} \times \{0\}^2$ with $\boldsymbol{x}_j \in B\mathbb{T} \times \mathbb{R}^2$. Thereby, we denote the torus $\mathbb{T}$ by $\mathbb{T} := \mathbb{R}/\mathbb{Z} \simeq [-1/2, 1/2)$. For a graphical illustration see Figure 1.1.

The Ewald formulas for 2d-periodic as well as for 1d-periodic geometries were already proposed in [18] and [32], respectively, and form the basis of the algorithms proposed in this paper. In contrast to the case of 3d-periodic boundary conditions, the application of the Ewald formulas for mixed periodic systems does not straightforwardly lead to fast algorithms. Some Fourier based algorithms, like MMM2D, MMM1D or ELC, see [6, 8, 7] and the fast and spectrally accurate Ewald summation in slab geometry [27], already exist, see also [37, 10, 9] for algorithms with higher complexity.

For open boundary conditions, i.e., $\mathcal{S} := \{0\}^3$ in (1.3), fast Fourier based methods [33, 34] where suggested, too. The relation of the Fourier based algorithms for open and 3d-periodic

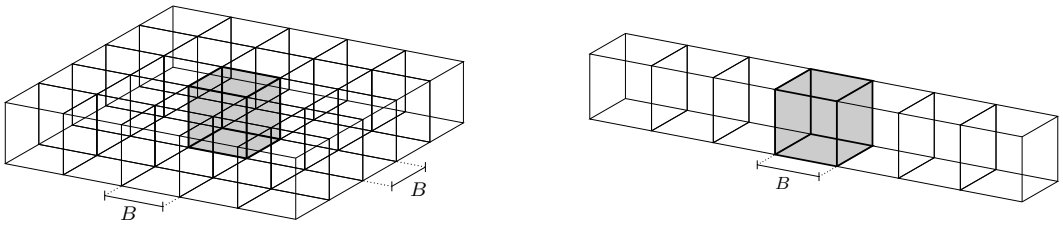

Figure 1.1: The simulation box is duplicated along two of three dimensions in the 2d-periodic case (left) and along one dimension in the 1d-periodic setting (right).

boundary conditions were already investigated in [30]. In this paper we aim to close the gap and propose FFT based algorithms also for 2d- and 1d-periodic boundary conditions. This approach was already proposed in the short paper [29]. In this paper we also present numerical results, show that the performance of the new algorithms is similar to the 3d-periodic case and go into detail about our implementation. Furthermore, we derive the Ewald formulas for 2d- and 1d-periodic systems, see Theorem 4.1 and Theorem 5.2, respectively. Thereby, we always start with the splitting (1.5) and then use the technique of convergence factors to derive the Fourier space representation of the long range part by applying the Poisson summation formula. We show that the obtained formulas can be used in order to derive the related algorithms, see Algorithm 4.3 and Algorithm 5.5. The main advantage of our approach is that the new algorithms are completely of the same structure as the well known algorithms for fully periodic and open boundary conditions, see [30]. That is that the short range parts of the potentials are computed directly and the long range parts are computed by an adjoint NFFT, followed by a multiplication in Fourier domain and again an NFFT in three dimensions, see Remark 4.4 and Remark 5.6.

As the paper contains numerical results we introduce the relative root mean square (rms) error in the fields, which is given by

$$\Delta E_{\mathcal{S}} := \left(\frac{\sum_{j=1}^{N} \left\| \boldsymbol{E}_{\mathcal{S}}(\boldsymbol{x}_j) - \tilde{\boldsymbol{E}}_{\mathcal{S}}(\boldsymbol{x}_j) \right\|^2}{\sum_{j=1}^{N} \left\| \boldsymbol{E}_{\mathcal{S}}(\boldsymbol{x}_j) \right\|^2} \right)^{1/2}, \tag{1.7}$$

where $\tilde{\boldsymbol{E}}_{\mathcal{S}}(\boldsymbol{x}_j)$ is some approximation of $\boldsymbol{E}_{\mathcal{S}}(\boldsymbol{x}_j)$, defined in (1.4). This error is often taken as a measure of accuracy. We remark that the fast multipole method can also handle all mentioned types of boundary conditions very efficiently, see [23, 22]. In order to estimate the rms field error in our numerical tests we used reference data computed with the fast multipole method for mixed periodic constraints.

The outline of this paper is as follows. We start with a short introduction to the non-equispaced fast Fourier transform (NFFT) in Section 2 and review the idea of fast Ewald summation based on NFFTs for 3d-periodic systems in Section 3. In Section 4 we consider the case of periodic boundary conditions in two of three dimensions. To this end, we introduce and prove the 2d-Ewald formulas, see Subsection 4.1, and develop a new fast algorithm in Subsection 4.2 for 2d-periodic systems. Furthermore, we present numerical results in Subsection 4.3, which show its efficiency. In order to rate the very good performance of the new algorithm, we compare the method to the particle-particle NFFT ($\mathrm{P^2NFFT}$) method for

3d-periodic systems [31]. Note that this algorithm is highly optimized and recently compared with other methods, such as the particle-particle particle-mesh (P^3M) method, the fast multipole method or multigrid based methods, see [5]. The 1d-periodic case is considered in an analog manner in Section 5. We present the 1d-Ewald formulas, see Subsection 5.1, develop a new fast algorithm in Subsection 5.2 for 1d-periodic systems and present numerical results in Subsection 5.3. Finally, we conclude with a short summary.

2. Prerequisite and NFFT

In this section we introduce the main notation and give a short introduction to the NFFT in three variables. To keep the notation short we define for some $\boldsymbol{M} = (M_1, \ldots, M_d) \in 2\mathbb{N}^d$ the index set $\mathcal{I}_{\boldsymbol{M}}$ by

$$\mathcal{I}_{\boldsymbol{M}} := \bigotimes_{j=1}^{d} \mathcal{I}_{M_j} \text{ , where } \mathcal{I}_{M_j} := \left\{ -\tfrac{M_j}{2}, \ldots, \tfrac{M_j}{2} - 1 \right\},$$

and the cardinality by $|\mathcal{I}_{\boldsymbol{M}}| := \prod_{j=1}^{d} M_j$. We do not distinguish between row and column vectors and denote by $\boldsymbol{x} \cdot \boldsymbol{y} := x_1y_1 + x_2y_2 + x_3y_3$ the scalar product and by $\boldsymbol{x} \odot \boldsymbol{y} := (x_1y_1, x_2y_2, x_3y_3) \in \mathbb{R}^3$ the component wise product of two vectors $\boldsymbol{x}, \boldsymbol{y} \in \mathbb{R}^3$. For some $\boldsymbol{x} \in \mathbb{R}^3$ with non-vanishing components we further define the vector $\boldsymbol{x}^{-1} := (x_1^{-1}, x_2^{-1}, x_3^{-1}) \in \mathbb{R}^3$.

Let a trigonometric polynomial $f\colon \mathbb{T}^3 \to \mathbb{C}$ be given by

$$f(\boldsymbol{x}) = \sum_{\boldsymbol{k} \in \mathcal{I}_{\boldsymbol{M}}} \hat{f}_{\boldsymbol{k}} \mathrm{e}^{-2\pi \mathrm{i} \boldsymbol{k} \cdot \boldsymbol{x}}, \tag{2.1}$$

with the Fourier coefficients $\hat{f}_{\boldsymbol{k}} \in \mathbb{C}$, $\boldsymbol{k} \in \mathcal{I}_{\boldsymbol{M}}$. The fast evaluation of f at arbitrarily chosen nodes $\boldsymbol{x}_j \in \mathbb{T}^3$, $j = 1, \ldots, N \in \mathbb{N}$, i.e., the efficient computation of

$$f_j := f(\boldsymbol{x}_j) = \sum_{\boldsymbol{k} \in \mathcal{I}_{\boldsymbol{M}}} \hat{f}_{\boldsymbol{k}} \mathrm{e}^{-2\pi \mathrm{i} \boldsymbol{k} \cdot \boldsymbol{x}_j}, \quad j = 1, \ldots, N, \tag{2.2}$$

is known as three-dimensional NFFT. We take the approach from [33] and approximate the trigonometric polynomial f by a sum of translates of a one-periodic function $\tilde{\varphi}$, which is defined via a tensor product of the periodization of a univariate window function φ, i.e., we set $\tilde{\varphi}_1(x) := \sum_{j=-\infty}^{\infty} \varphi(x+j)$ and define the trivariate function $\tilde{\varphi}$ by $\tilde{\varphi}(\boldsymbol{x}) := \tilde{\varphi}_1(x_1) \cdot \tilde{\varphi}_1(x_2) \cdot \tilde{\varphi}_1(x_3)$. We obtain

$$f(\boldsymbol{x}) \approx \sum_{\boldsymbol{l} \in \mathcal{I}_{\boldsymbol{m}}} g_{\boldsymbol{l}} \tilde{\varphi}(\boldsymbol{x} - \boldsymbol{l} \odot \boldsymbol{m}^{-1}), \tag{2.3}$$

where we choose $\boldsymbol{M} \leq \boldsymbol{m} \in 2\mathbb{N}^3$ (component wise). Furthermore, the function $\tilde{\varphi}$ is assumed to be well localized in spatial and frequency domain. Under these assumptions, it can be shown that

$$g_{\boldsymbol{l}} := \frac{1}{|\mathcal{I}_{\boldsymbol{m}}|} \sum_{\boldsymbol{k} \in \mathcal{I}_{\boldsymbol{M}}} \frac{\hat{f}_{\boldsymbol{k}}}{c_{\boldsymbol{k}}(\tilde{\varphi})} \mathrm{e}^{2\pi \mathrm{i} \boldsymbol{k} \cdot (\boldsymbol{l} \odot \boldsymbol{m}^{-1})}$$

is a reasonable choice of the unknown coefficients in (2.3), where $c_{\boldsymbol{k}}(\tilde{\varphi})$ denotes the $\boldsymbol{k}$-th Fourier coefficient of $\tilde{\varphi}$. After calculating the coefficients $g_{\boldsymbol{l}}$ by an FFT the function values f_j are computed via (2.3), where the sums are short due to the good localization of $\tilde{\varphi}$ in spatial

domain. The adjoint nonequispaced fast Fourier transform ($\mathrm{NFFT}^{\mathrm{H}}$) is an algorithm for the fast evaluation of

$$\hat{h}_{\boldsymbol{k}} = \sum_{j=1}^{N} f_j \mathrm{e}^{2\pi \mathrm{i} \boldsymbol{k}\cdot\boldsymbol{x}_j}, \qquad \boldsymbol{k} \in \mathcal{I}_{\boldsymbol{M}}, \tag{2.4}$$

where now the coefficients $f_j \in \mathbb{C}$ are given. Both algorithms have very similar structures and can be performed in $\mathcal{O}(|\mathcal{I}_{\boldsymbol{M}}| \log |\mathcal{I}_{\boldsymbol{M}}| + N)$ arithmetic operations, see [35, 24].

3. Fast Ewald summation for 3d–periodic boundary conditions

For an electrical neutral system of N charges q_j distributed in a cubic box of edge length B we define the electrostatic potential subject to 3d–periodic boundary conditions by

$$\phi^{\mathrm{p3}}(\boldsymbol{x}_j) := \phi_{\mathbb{Z}^3}(\boldsymbol{x}_j) = \sum_{s=0}^{\infty} \sum_{\substack{\boldsymbol{n}\in\mathbb{Z}^3 \\ \|\boldsymbol{n}\|^2=s}} {\sum_{i=1}^{N}}' \frac{q_i}{\|\boldsymbol{x}_{ij} + B\boldsymbol{n}\|}, \tag{3.1}$$

i.e., we set $\mathcal{S} := \mathbb{Z}^3$ within the definitions (1.2) – (1.4) and apply a spherical order of summation. We obtain [16, 25]

$$\phi^{\mathrm{p3}}(\boldsymbol{x}_j) = \phi^{\mathrm{p3,S}}(\boldsymbol{x}_j) + \phi^{\mathrm{p3,L}}(\boldsymbol{x}_j) + \phi^{\mathrm{p3,self}}(\boldsymbol{x}_j), \tag{3.2}$$

where for the splitting parameter $\alpha > 0$ we define the short range part

$$\phi^{\mathrm{p3,S}}(\boldsymbol{x}_j) := \sum_{\boldsymbol{n}\in\mathbb{Z}^3} {\sum_{i=1}^{N}}' q_i \frac{\operatorname{erfc}(\alpha\|\boldsymbol{x}_{ij} + B\boldsymbol{n}\|)}{\|\boldsymbol{x}_{ij} + B\boldsymbol{n}\|},$$

the long range part

$$\phi^{\mathrm{p3,L}}(\boldsymbol{x}_j) := \frac{1}{\pi B} \sum_{\boldsymbol{k}\in\mathbb{Z}^3\setminus\{\boldsymbol{0}\}} \frac{\mathrm{e}^{-\pi^2\|\boldsymbol{k}\|^2/(\alpha^2 B^2)}}{\|\boldsymbol{k}\|^2} \left(\sum_{i=1}^{N} q_i \mathrm{e}^{2\pi\mathrm{i}\boldsymbol{k}\cdot\boldsymbol{x}_i/B} \right) \mathrm{e}^{-2\pi\mathrm{i}\boldsymbol{k}\cdot\boldsymbol{x}_j/B},$$

and the self potential

$$\phi^{\mathrm{p3,self}}(\boldsymbol{x}_j) := -\frac{2\alpha}{\sqrt{\pi}} q_j.$$

Often a fourth term, the so called dipole correction term, appears in the decomposition (3.2), cf. [13]. The dipole correction term is the only part depending on the order of summation. However, if a spherical summation order is applied, the dipole correction term depends only on the norm of the dipole moment $\sum_{j=1}^{N} q_j \boldsymbol{x}_j$ and, additionally, on the dielectric constant of the surrounding medium. Therefore, it can be computed efficiently in $\mathcal{O}(N)$ arithmetic operations. If the medium is assumed to be metallic, the dipole term vanishes and (3.2) applies. It should be mentioned that the formulas above can be generalized to non-cubic boxes and also non-orthogonal (triclinic) boxes, cf. [16, 12, 21]. As the complementary error function erfc rapidly tends to zero, the short range part of each potential $\phi^{\mathrm{p3,S}}(\boldsymbol{x}_j)$ can be

obtained by direct evaluation. In order to compute the long range parts $\phi^{\mathrm{p3,L}}(\boldsymbol{x}_j)$ we truncate the infinite sum and compute approximations of the sums

$$\hat{S}(\boldsymbol{k}) := \sum_{i=1}^{N} q_i \mathrm{e}^{2\pi \mathrm{i} \boldsymbol{k}\cdot\boldsymbol{x}_i/B}, \quad \boldsymbol{k} \in \mathcal{I}_{\boldsymbol{M}},$$

with an adjoint NFFT and evaluate

$$\phi^{\mathrm{p3,L}}(\boldsymbol{x}_j) \approx \frac{1}{\pi B} \sum_{\boldsymbol{k}\in\mathcal{I}_{\boldsymbol{M}}\setminus\{\boldsymbol{0}\}} \hat{b}_{\boldsymbol{k}} \hat{S}(\boldsymbol{k}) \mathrm{e}^{-2\pi \mathrm{i} \boldsymbol{k}\cdot\boldsymbol{x}_j/B}, \quad j = 1, \ldots, N,$$

where we define the Fourier coefficients

$$\hat{b}_{\boldsymbol{k}} := \frac{\mathrm{e}^{-\pi^2\|\boldsymbol{k}\|^2/\alpha^2 B^2}}{\|\boldsymbol{k}\|^2}, \tag{3.3}$$

via the NFFT. In matrix vector notation we may write

$$\Big(\phi^{\mathrm{p3,L}}(\boldsymbol{x}_j)\Big)_{j=1}^{N} \approx \mathcal{A}\mathcal{D}\mathcal{A}^{\mathsf{H}}\boldsymbol{q}, \tag{3.4}$$

where $\mathcal{A}$ denotes the matrix representation of the NFFT in three dimensions, $\mathcal{D}$ is a diagonal matrix with entries $\frac{1}{\pi B}\hat{b}_{\boldsymbol{k}}$, $\boldsymbol{k} \in \mathcal{I}_{\boldsymbol{M}}$, and $\boldsymbol{q} = (q_1, \ldots, q_N)^{\top} \in \mathbb{R}^N$.

The force acting on a particle j can be written as

$$\boldsymbol{F}^{\mathrm{p3}}(\boldsymbol{x}_j) = \boldsymbol{F}^{\mathrm{p3,S}}(\boldsymbol{x}_j) + \boldsymbol{F}^{\mathrm{p3,L}}(\boldsymbol{x}_j) := -q_j \nabla \phi^{\mathrm{p3,S}}(\boldsymbol{x}_j) - q_j \nabla \phi^{\mathrm{p3,L}}(\boldsymbol{x}_j),$$

where the short range part $\boldsymbol{F}^{\mathrm{p3,S}}(\boldsymbol{x}_j)$ is given by

$$\boldsymbol{F}^{\mathrm{S}}_{\mathcal{S}}(\boldsymbol{x}_j) := -q_j \sum_{\boldsymbol{n}\in\mathcal{S}} {\sum_{i=1}^{N}}' q_i \left(\frac{2\alpha}{\sqrt{\pi}} \mathrm{e}^{-\alpha^2\|\boldsymbol{x}_{ij}+B\boldsymbol{n}\|^2} + \frac{\operatorname{erfc}(\alpha\|\boldsymbol{x}_{ij}+B\boldsymbol{n}\|)}{\|\boldsymbol{x}_{ij}+B\boldsymbol{n}\|} \right) \frac{\boldsymbol{x}_{ij}+B\boldsymbol{n}}{\|\boldsymbol{x}_{ij}+B\boldsymbol{n}\|^2} \tag{3.5}$$

with $\mathcal{S} := \mathbb{Z}^3$ and can be evaluated by direct summation, too. The long range part can be obtained by differentiation in Fourier space, i.e., we write

$$\boldsymbol{F}^{\mathrm{p3,L}}(\boldsymbol{x}_j) = \frac{2\mathrm{i}q_j}{B^2} \sum_{\boldsymbol{k}\in\mathbb{Z}^3\setminus\{\boldsymbol{0}\}} \hat{b}_{\boldsymbol{k}} \boldsymbol{k} \hat{S}(\boldsymbol{k}) \mathrm{e}^{-2\pi \mathrm{i} \boldsymbol{k}\cdot\boldsymbol{x}_j/B}$$

and use a NFFT in each dimension for an efficient evaluation. This approach is widely known as i$\boldsymbol{k}$ differentiation, see [13] for instance. An alternative is the so called analytic differentiation approach [12], where the ∇ operator is applied to the NFFT window function. In terms of (2.1) and (2.3) this means that we set

$$\hat{f}_{\boldsymbol{k}} := \begin{cases} \hat{b}_{\boldsymbol{k}} \hat{S}(\boldsymbol{k}) & : \boldsymbol{k} \neq \boldsymbol{0}, \\ 0 & : \boldsymbol{k} = \boldsymbol{0} \end{cases}$$

and compute the long range portion of the force $\boldsymbol{F}^{\mathrm{p3}}(\boldsymbol{x}_j)$ by

$$\boldsymbol{F}^{\mathrm{p3,L}}(\boldsymbol{x}_j) \approx -\frac{q_j}{\pi B} \sum_{\boldsymbol{l}\in\mathcal{I}_{\boldsymbol{m}}} g_{\boldsymbol{l}} \nabla \tilde{\varphi}(\boldsymbol{x}_j - \boldsymbol{l} \odot \boldsymbol{m}^{-1}). \tag{3.6}$$

4. Fast Ewald summation for 2d-periodic boundary conditions

4.1. Ewald summation

We consider a system of N charges $q_j \in \mathbb{R}$ at positions $\boldsymbol{x}_j \in B\mathbb{T}^2 \times \mathbb{R}$. Under periodic boundary conditions in the first two dimensions we define the potential of each single particle by

$$\phi^{\mathrm{p2}}(\boldsymbol{x}_j) := \phi_{\mathbb{Z}^2\times\{0\}}(\boldsymbol{x}_j) = \sum_{s=0}^{\infty} \sum_{\substack{\boldsymbol{n}\in\mathbb{Z}^2\times\{0\} \\ \|\boldsymbol{n}\|^2=s}} \sum_{i=1}^{N}{}' \frac{q_i}{\|\boldsymbol{x}_{ij} + B\boldsymbol{n}\|} \tag{4.1}$$

and define the Coulomb energy via

$$U^{\mathrm{p2}} := U_{\mathbb{Z}^2\times\{0\}} = \frac{1}{2}\sum_{j=1}^{N} q_j \phi^{\mathrm{p2}}(\boldsymbol{x}_j), \tag{4.2}$$

i.e., we set $\mathcal{S} := \mathbb{Z}^2 \times \{0\}$ in (1.2) – (1.4) and use the spherical limit as in (3.1).

In the following theorem we consider the 2d-Ewald formula, see [18], and give a proof using convergence factors, similar to [25], where the 3d-periodic case is treated. In this section we denote for $\boldsymbol{y} \in \mathbb{R}^3$ the vector of its first two components by $\tilde{\boldsymbol{y}} := (y_1, y_2) \in \mathbb{R}^2$.

Theorem 4.1. *Consider an electrical neutral system of N charges $q_j \in \mathbb{R}$ at positions $\boldsymbol{x}_j = (\tilde{\boldsymbol{x}}_j, x_{j,3}) \in B\mathbb{T}^2 \times \mathbb{R}$, $j = 1, \dots, N$. Under periodic boundary conditions in the first two variables the potentials $\phi^{\mathrm{p2}}(\boldsymbol{x}_j)$, defined in* (4.1)*, can be written in the form*

$$\phi^{\mathrm{p2}}(\boldsymbol{x}_j) = \phi^{\mathrm{p2,S}}(\boldsymbol{x}_j) + \phi^{\mathrm{p2,L}}(\boldsymbol{x}_j) + \phi^{\mathrm{p2},\mathbf{0}}(\boldsymbol{x}_j) + \phi^{\mathrm{p2,self}}(\boldsymbol{x}_j),$$

where for some $\alpha > 0$ we define the short range part

$$\phi^{\mathrm{p2,S}}(\boldsymbol{x}_j) := \sum_{\boldsymbol{n}\in\mathbb{Z}^2\times\{0\}} \sum_{i=1}^{N}{}' q_i \frac{\operatorname{erfc}(\alpha\|\boldsymbol{x}_{ij} + B\boldsymbol{n}\|)}{\|\boldsymbol{x}_{ij} + B\boldsymbol{n}\|}, \tag{4.3}$$

the long range parts

$$\phi^{\mathrm{p2,L}}(\boldsymbol{x}_j) := \frac{1}{2B} \sum_{\boldsymbol{k}\in\mathbb{Z}^2\setminus\{\mathbf{0}\}} \sum_{i=1}^{N} q_i \, \mathrm{e}^{2\pi i \boldsymbol{k}\cdot\tilde{\boldsymbol{x}}_{ij}/B} \cdot \Theta^{\mathrm{p2}}(\|\boldsymbol{k}\|, x_{ij,3}),$$

$$\phi^{\mathrm{p2},\mathbf{0}}(\boldsymbol{x}_j) := -\frac{2\sqrt{\pi}}{B^2} \sum_{i=1}^{N} q_i \left(\frac{\mathrm{e}^{-\alpha^2 x_{ij,3}^2}}{\alpha} + \sqrt{\pi} x_{ij,3} \operatorname{erf}(\alpha x_{ij,3}) \right),$$

the self potential

$$\phi^{\mathrm{p2,self}}(\boldsymbol{x}_j) := -\frac{2\alpha}{\sqrt{\pi}} q_j \ ,$$

and the function $\Theta^{\mathrm{p2}}(k, r)$ for $k, r \in \mathbb{R}$ is defined by

$$\Theta^{\mathrm{p2}}(k, r) := \frac{1}{k} \left[\mathrm{e}^{2\pi k r/B} \operatorname{erfc}\left(\frac{\pi k}{\alpha B} + \alpha r \right) + \mathrm{e}^{-2\pi k r/B} \operatorname{erfc}\left(\frac{\pi k}{\alpha B} - \alpha r \right) \right]. \tag{4.4}$$

Proof. In contrast to the case of periodicity in all three dimensions, it can be shown that a convergence factor of the form $\mathrm{e}^{-s\|\boldsymbol{x}_{ij}+B\boldsymbol{n}\|}$ instead of $\mathrm{e}^{-s\|B\boldsymbol{n}\|}$ can be used in order to calculate the spherical limit (4.1). For a proof see [6] or [4]. Thereby, the factor $\mathrm{e}^{-s\|\boldsymbol{x}_{ij}+B\boldsymbol{n}\|}$ can be replaced by $\mathrm{e}^{-s\|\boldsymbol{x}_{ij}+B\boldsymbol{n}\|^2}$.

As in [28] we apply the convergence factor $\mathrm{e}^{-s\|\boldsymbol{x}_{ij}+B\boldsymbol{n}\|^2}$ for the calculation of the potential (3.1), i.e., we compute the limit

$$\phi^{\mathrm{p2}}(\boldsymbol{x}_j) = \lim_{s\to 0} \sum_{\boldsymbol{n}\in\mathbb{Z}^2\times\{0\}} {\sum_{i=1}^{N}}' \frac{q_i \mathrm{e}^{-s\|\boldsymbol{x}_{ij}+B\boldsymbol{n}\|^2}}{\|\boldsymbol{x}_{ij}+B\boldsymbol{n}\|}.$$

For the calculation of $\phi^{\mathrm{p2}}(\boldsymbol{x}_j)$ we first apply (1.5) for the splitting parameter $\alpha > 0$ and obtain by exploiting (1.6)

$$\phi^{\mathrm{p2}}(\boldsymbol{x}_j) = \phi^{\mathrm{p2,S}}(\boldsymbol{x}_j) + \sum_{\boldsymbol{n}\in\mathbb{Z}^2\times\{0\}} \sum_{i=1}^{N} q_i \frac{\mathrm{erf}(\alpha\|\boldsymbol{x}_{ij}+B\boldsymbol{n}\|)}{\|\boldsymbol{x}_{ij}+B\boldsymbol{n}\|} + \phi^{\mathrm{p2,self}}(\boldsymbol{x}_j).$$

In order to calculate the remaining long range part we define

$$\phi_s(\boldsymbol{x}_j) := \sum_{\boldsymbol{n}\in\mathbb{Z}^2\times\{0\}} \sum_{i=1}^{N} q_i \mathrm{e}^{-s\|\boldsymbol{x}_{ij}+B\boldsymbol{n}\|^2} \frac{\mathrm{erf}(\alpha\|\boldsymbol{x}_{ij}+B\boldsymbol{n}\|)}{\|\boldsymbol{x}_{ij}+B\boldsymbol{n}\|},$$

which is absolutely convergent for all $s > 0$ and uniformly convergent on $s \geq 0$, cf. [25]. Then, we consider the limit $\lim_{s\to 0} \phi_s(\boldsymbol{x}_j)$. In the following, we apply the identity

$$\mathrm{erf}(\alpha\|\boldsymbol{x}_{ij}+B\boldsymbol{n}\|) = \frac{2}{\sqrt{\pi}}\|\boldsymbol{x}_{ij}+B\boldsymbol{n}\| \int_0^{\alpha} \mathrm{e}^{-\|\boldsymbol{x}_{ij}+B\boldsymbol{n}\|^2 z^2} \mathrm{d}z \tag{4.5}$$

in $\phi_s(\boldsymbol{x}_j)$ and use the Poisson summation formula

$$\sum_{\boldsymbol{n}\in\mathbb{Z}^2} \mathrm{e}^{-\beta\|\boldsymbol{x}+B\boldsymbol{n}\|^2} = \frac{1}{B^2} \sum_{\boldsymbol{k}\in\mathbb{Z}^2} \frac{\pi}{\beta} \mathrm{e}^{-\pi^2\|\boldsymbol{k}\|^2/(B^2\beta)} \mathrm{e}^{2\pi\mathrm{i}\boldsymbol{k}\cdot\boldsymbol{x}/B}$$

for a Gaussian kernel in two variables, which is valid for $\beta > 0$ and uniformly convergent on $\mathbb{R}^2$. Applying (4.5) we can write $\phi_s(\boldsymbol{x}_j)$ for $s > 0$ as an absolutely and uniformly convergent sum of absolutely and uniformly convergent integrals. Thus, we may change the order of summation and integration to get

$$\begin{aligned}
\phi_s(\boldsymbol{x}_j) &= \frac{2}{\sqrt{\pi}} \int_0^{\alpha} \sum_{i=1}^{N} q_i \mathrm{e}^{-(s+z^2)x_{ij,3}^2} \sum_{\tilde{\boldsymbol{n}}\in\mathbb{Z}^2} \mathrm{e}^{-(s+z^2)\|\tilde{\boldsymbol{x}}_{ij}+B\tilde{\boldsymbol{n}}\|^2} \mathrm{d}z \\
&= \frac{2}{\sqrt{\pi}} \int_0^{\alpha} \sum_{i=1}^{N} q_i \mathrm{e}^{-(s+z^2)x_{ij,3}^2} \sum_{\boldsymbol{k}\in\mathbb{Z}^2} \frac{\pi}{B^2(s+z^2)} \mathrm{e}^{\frac{-\pi^2\|\boldsymbol{k}\|^2}{B^2(s+z^2)}} \mathrm{e}^{2\pi\mathrm{i}\boldsymbol{k}\cdot\tilde{\boldsymbol{x}}_{ij}/B} \mathrm{d}z.
\end{aligned}$$

As the Fourier series is uniformly convergent and the terms of the sum are continuous functions on $[0, \alpha]$ we obtain

$$\phi_s(\boldsymbol{x}_j) = \frac{2}{\sqrt{\pi}} \sum_{\boldsymbol{k}\in\mathbb{Z}^2} \sum_{i=1}^{N} q_i \frac{\pi}{B^2} \mathrm{e}^{2\pi\mathrm{i}\boldsymbol{k}\cdot\tilde{\boldsymbol{x}}_{ij}/B} \int_0^{\alpha} \frac{1}{s+z^2} \mathrm{e}^{\frac{-\pi^2\|\boldsymbol{k}\|^2}{B^2(s+z^2)}} \mathrm{e}^{-x_{ij,3}^2(s+z^2)} \mathrm{d}z. \tag{4.6}$$

In the following we separate the $\boldsymbol{k} = \mathbf{0}$ term and consider the sum

$$\frac{2}{\sqrt{\pi}} \sum_{\boldsymbol{k}\in\mathbb{Z}^2\setminus\{\mathbf{0}\}} \sum_{i=1}^{N} q_i \frac{\pi}{B^2} \mathrm{e}^{2\pi \mathrm{i}\boldsymbol{k}\cdot\tilde{\boldsymbol{x}}_{ij}/B} \int_0^\alpha \frac{1}{s+z^2} \mathrm{e}^{\frac{-\pi^2\|\boldsymbol{k}\|^2}{B^2(s+z^2)}} \mathrm{e}^{-x_{ij,3}^2(s+z^2)} \mathrm{d}z.$$

If the limit for $s \to 0$ of each single summand exists, we are allowed to change the order of summation and calculating the limits. In the following, we will show that these limits exist. We have

$$\lim_{s\to 0} \int_0^\alpha \frac{1}{s+z^2} \mathrm{e}^{\frac{-\pi^2\|\boldsymbol{k}\|^2}{B^2(s+z^2)}} \mathrm{e}^{-x_{ij,3}^2(s+z^2)} \mathrm{d}z = \int_0^\alpha \frac{1}{z^2} \mathrm{e}^{\frac{-\pi^2\|\boldsymbol{k}\|^2}{B^2 z^2}} \mathrm{e}^{-x_{ij,3}^2 z^2} \mathrm{d}z.$$

This can be proved as follows. For $s > 0$ we define the function f_s by $f_s(z) := z^2 + s$ and set $f(z) := z^2$. Then the convergence $f_s \to f$ is uniform on $[0, \alpha]$. The function

$$h(y) := \begin{cases} \frac{1}{y} \mathrm{e}^{\frac{-\pi^2\|\boldsymbol{k}\|^2}{B^2 y}} \mathrm{e}^{-x_{ij,3}^2 y} & : z \neq 0, \\ 0 & : z = 0 \end{cases}$$

is continuous and, therefore, uniformly continuous on $[0, \alpha]$. Thus, the convergence $h \circ f_s \to h \circ f$ is also uniform on $[0, \alpha]$ and the limit can be applied to the integrand. For the computation of the integral on the right hand side we substitute $y := z^{-1}$ and obtain

$$\begin{aligned} \int_0^\alpha \frac{1}{z^2} \mathrm{e}^{\frac{-\pi^2\|\boldsymbol{k}\|^2}{B^2 z^2}} \mathrm{e}^{-x_{ij,3}^2 z^2} \mathrm{d}z &= \int_{1/\alpha}^\infty \exp\left(\frac{-\pi^2\|\boldsymbol{k}\|^2 y^2}{B^2} - \frac{x_{ij,3}^2}{y^2} \right) \mathrm{d}y \\ &= \int_{1/\alpha}^\infty \exp\left[-\left(\frac{\pi\|\boldsymbol{k}\| y}{B} + \frac{x_{ij,3}}{y} \right)^2 + \frac{2\pi\|\boldsymbol{k}\| x_{ij,3}}{B} \right] \mathrm{d}y \qquad (4.7) \\ &= \int_{1/\alpha}^\infty \exp\left[-\left(\frac{\pi\|\boldsymbol{k}\| y}{B} - \frac{x_{ij,3}}{y} \right)^2 - \frac{2\pi\|\boldsymbol{k}\| x_{ij,3}}{B} \right] \mathrm{d}y. \qquad (4.8) \end{aligned}$$

For the substitutions

$$t_1 := \frac{\pi\|\boldsymbol{k}\| y}{B} + \frac{x_{ij,3}}{y} \quad \text{and} \quad t_2 := \frac{\pi\|\boldsymbol{k}\| y}{B} - \frac{x_{ij,3}}{y}$$

we obtain

$$\mathrm{d}t_1 + \mathrm{d}t_2 = \left(\frac{\pi\|\boldsymbol{k}\|}{B} - \frac{x_{ij,3}}{y^2} \right) \mathrm{d}y + \left(\frac{\pi\|\boldsymbol{k}\|}{B} + \frac{x_{ij,3}}{y^2} \right) \mathrm{d}y = \frac{2\pi\|\boldsymbol{k}\|}{B} \mathrm{d}y.$$

Thus, using (4.7) and (4.8), we get

$$\begin{aligned} \int_0^\alpha \frac{1}{z^2} \mathrm{e}^{\frac{-\pi^2\|\boldsymbol{k}\|^2}{B^2 z^2}} \mathrm{e}^{-x_{ij,3}^2 z^2} \mathrm{d}z = \frac{B}{2\pi\|\boldsymbol{k}\|} \Bigg[& \mathrm{e}^{2\pi\|\boldsymbol{k}\| x_{ij,3}/B} \int_{\frac{\pi\|\boldsymbol{k}\|}{\alpha B} + \alpha x_{ij,3}}^\infty \mathrm{e}^{-t_1^2} \mathrm{d}t_1 \\ & + \mathrm{e}^{-2\pi\|\boldsymbol{k}\| x_{ij,3}/B} \int_{\frac{\pi\|\boldsymbol{k}\|}{\alpha B} - \alpha x_{ij,3}}^\infty \mathrm{e}^{-t_2^2} \mathrm{d}t_2 \Bigg] = \frac{B\sqrt{\pi}}{4\pi} \Theta^{\mathrm{p2}}(\|\boldsymbol{k}\|, x_{ij,3}) \end{aligned}$$

and, therefore, the limit of $\phi_s(\boldsymbol{x}_j)$ can be written in the form

$$\lim_{s\to 0} \phi_s(\boldsymbol{x}_j) = \phi^{\mathrm{p2,L}}(\boldsymbol{x}_j) + \lim_{s\to 0} \frac{2\sqrt{\pi}}{B^2} \sum_{i=1}^{N} q_i \mathrm{e}^{-s x_{ij,3}^2} \int_0^\alpha \frac{\mathrm{e}^{-x_{ij,3}^2 z^2}}{s+z^2} \mathrm{d}z.$$

Now, we use the substitution $y := \frac{z}{\sqrt{s}}$ and obtain

$$I(s) := \int_0^{\alpha} \frac{\mathrm{e}^{-x_{ij,3}^2 z^2}}{s+z^2}\mathrm{d}z = \int_0^{\frac{\alpha}{\sqrt{s}}} \frac{\mathrm{e}^{-s x_{ij,3}^2 z^2}}{\sqrt{s}(1+z^2)}\mathrm{d}z.$$

Replacing the term $f(s) := \mathrm{e}^{-s x_{ij,3}^2 z^2}$ by its Taylor representation $f(s) = \sum_{n=0}^{\infty} (-1)^n (x_{ij,3} z)^{2n} \frac{s^n}{n!}$ we have

$$I(s) = \sum_{n=0}^{\infty} \frac{(-1)^n x_{ij,3}^{2n} s^n}{n!\sqrt{s}} \int_0^{\frac{\alpha}{\sqrt{s}}} \frac{z^{2n}}{1+z^2}\mathrm{d}z. \tag{4.9}$$

In the following steps we make use of the identity

$$\int_0^{\beta} \frac{z^{2n}}{1+z^2}\mathrm{d}z = (-1)^n \arctan\beta + (-1)^{n+1} \sum_{k=0}^{n-1} (-1)^k \frac{\beta^{2k+1}}{2k+1}, \tag{4.10}$$

which is valid for $\beta > 0$, $n \in \mathbb{N}_0$ and can easily be verified by induction. Furthermore, we use the Taylor representation

$$\sqrt{\pi}\alpha z \cdot \operatorname{erf}(\alpha z) + \mathrm{e}^{-\alpha^2 z^2} = 1 + \sum_{n=0}^{\infty} \frac{(-1)^n (\alpha z)^{2n+2}}{(n+1)!(2n+1)}$$

holding for $\alpha > 0$ and each $z \in \mathbb{R}$. Applying (4.10) with $\beta = \frac{\alpha}{\sqrt{s}}$ we get

$$\begin{aligned}
\frac{s^n}{\sqrt{s}} \int_0^{\frac{\alpha}{\sqrt{s}}} \frac{z^{2n}}{1+z^2}\mathrm{d}z &= \frac{(-1)^n s^n}{\sqrt{s}} \arctan\left(\tfrac{\alpha}{\sqrt{s}}\right) + (-1)^{n+1} \sum_{k=0}^{n-1} (-1)^k \frac{\alpha^{2k+1} s^n}{(2k+1) s^{k+1}} \\
&= \begin{cases} \mathcal{O}(\sqrt{s}) + \frac{\alpha^{2n-1}}{(2n-1)} + \mathcal{O}(s) \text{ for } s \to 0 & : n > 0, \\ \frac{1}{\sqrt{s}} \arctan\left(\frac{\alpha}{\sqrt{s}}\right) & : n = 0. \end{cases}
\end{aligned}$$

Inserting this result into (4.9) we obtain

$$\begin{aligned}
I(s) &= \frac{1}{\sqrt{s}} \arctan\left(\tfrac{\alpha}{\sqrt{s}}\right) + \sum_{n=1}^{\infty} \frac{(-1)^n x_{ij}^{2n} \alpha^{2n-1}}{n!(2n-1)} + \mathcal{O}(\sqrt{s}) \\
&= \frac{1}{\sqrt{s}} \arctan\left(\tfrac{\alpha}{\sqrt{s}}\right) + \sum_{n=0}^{\infty} \frac{(-1)^{n+1} x_{ij}^{2n+2} \alpha^{2n+1}}{(n+1)!(2n+1)} + \mathcal{O}(\sqrt{s}) \\
&= \frac{1}{\sqrt{s}} \arctan\left(\tfrac{\alpha}{\sqrt{s}}\right) - \sqrt{\pi} x_{ij,3} \cdot \operatorname{erf}(\alpha x_{ij,3}) - \frac{1}{\alpha} \mathrm{e}^{-\alpha^2 x_{ij,3}^2} + \frac{1}{\alpha} + \mathcal{O}(\sqrt{s})
\end{aligned}$$

and by exploiting the charge neutrality (1.1) we get

$$\begin{aligned}
\lim_{s\to 0} \phi_s(\boldsymbol{x}_j) &= \phi^{\mathrm{p2,L}}(\boldsymbol{x}_j) + \lim_{s\to 0} \frac{2\sqrt{\pi}}{B^2} \sum_{i=1}^{N} q_i \mathrm{e}^{-s x_{ij,3}^2} I(s) \\
&= \phi^{\mathrm{p2,L}}(\boldsymbol{x}_j) - \frac{2\sqrt{\pi}}{B^2} \sum_{i=1}^{N} q_i \left(\frac{\mathrm{e}^{-\alpha^2 x_{ij,3}^2}}{\alpha} + \sqrt{\pi} x_{ij,3} \cdot \operatorname{erf}(\alpha x_{ij,3}) \right) \\
&= \phi^{\mathrm{p2,L}}(\boldsymbol{x}_j) + \phi^{\mathrm{p2},\mathbf{0}}(\boldsymbol{x}_j)\,.
\end{aligned}$$

■

With the following lemma we show that the function $\Theta^{\mathrm{p2}}(k,r)$ tends to zero exponentially fast with respect to k, i.e., we can truncate the infinite sum in $\phi^{\mathrm{p2,L}}(\boldsymbol{x}_j)$.

Lemma 4.2. *For arbitrary $r \in \mathbb{R}$ we have for the function Θ^{p2} given in* (4.4)

$$\Theta^{\mathrm{p2}}(k,r) \to 0 \text{ with } \Theta^{\mathrm{p2}}(k,r) = o(k^{-2}\mathrm{e}^{-k^2}) \text{ for } k \to \infty.$$

Proof. The function Θ^{p2} has the integral representation

$$\Theta^{\mathrm{p2}}(k,r) = \frac{4\sqrt{\pi}}{B} \int_0^\alpha \frac{1}{t^2} \exp\left(-\frac{\pi^2 k^2}{B^2 t^2} - r^2 t^2\right) \mathrm{d}t,$$

as we have seen in the proof of Theorem 4.1. Now, we easily see

$$\Theta^{\mathrm{p2}}(k,r) \leq \Theta^{\mathrm{p2}}(k,0) = \frac{2}{k} \operatorname{erfc}\left(\frac{\pi k}{\alpha B}\right) \approx \frac{2\alpha B}{k^2 \pi^{3/2}} \mathrm{e}^{-\frac{\pi^2 k^2}{\alpha^2 B^2}},$$

which is valid for large k, cf. [2, number 7.1.23]. ∎

4.2. Fast NFFT based algorithm for 2d-periodic systems

Based on Theorem 4.1 we derive a fast algorithm. The evaluation of the short range part $\phi^{\mathrm{p2,S}}(\boldsymbol{x}_j)$ is done by a direct evaluation. For the computation of the long range part we apply the fast summation method [33] to the functions $\Theta^{\mathrm{p2}}(k,\cdot)$.

4.2.1. Computational approach

Due to Lemma 4.2 we can truncate the infinite sum in $\phi^{\mathrm{p2,L}}(\boldsymbol{x}_j)$, i.e., for some appropriate $\tilde{\boldsymbol{M}} = (M_1, M_2) \in 2\mathbb{N}^2$ we set

$$\phi^{\mathrm{p2,L}}(\boldsymbol{x}_j) \approx \frac{1}{2B} \sum_{\boldsymbol{k} \in \mathcal{I}_{\tilde{\boldsymbol{M}}} \setminus \{\boldsymbol{0}\}} \sum_{i=1}^{N} q_i \mathrm{e}^{2\pi \mathrm{i} \boldsymbol{k} \cdot \tilde{\boldsymbol{x}}_{ij}/B} \Theta^{\mathrm{p2}}(\|\boldsymbol{k}\|, x_{ij,3}).$$

Note, that all the functions $\Theta^{\mathrm{p2}}(\|\boldsymbol{k}\|,\cdot)$ have to be evaluated only within a finite interval $[-B_3/2, B_3/2]$. The main idea is to approximate the functions $\Theta^{\mathrm{p2}}(\|\boldsymbol{k}\|,\cdot)$ on this interval by a truncated Fourier series. However, the odd derivatives of $\Theta^{\mathrm{p2}}(\|\boldsymbol{k}\|,\cdot)$ at the points $-B_3/2$ and $B_3/2$ do not match, which yields a bad convergence rate of the Fourier series. Therefore, we extend the interval at both ends, where we construct a smooth transition. In the following, we give the formal derivation of this idea.

Let $h > 0$ and $\varepsilon > 0$ such that $|x_{ij,3}| \leq h(1/2 - \varepsilon)$ for all $i, j = 1, \ldots, N$ and define

$$\Theta_0^{\mathrm{p2}}(r) := \frac{\mathrm{e}^{-\alpha^2 r^2}}{\alpha} + \sqrt{\pi} r \operatorname{erf}(\alpha r).$$

In order to approximate the long range parts $\phi^{\mathrm{p2,L}}(\boldsymbol{x}_j) + \phi^{\mathrm{p2},\boldsymbol{0}}(\boldsymbol{x}_j)$ efficiently we consider for $k \in \{\|\boldsymbol{k}\| : \boldsymbol{k} \in \mathcal{I}_{\tilde{\boldsymbol{M}}}\}$ the regularizations

$$K_{\mathrm{R}}(k,r) := \begin{cases} \dfrac{1}{2B}\Theta^{\mathrm{p2}}(k,r) & : k \neq 0, |h^{-1}r| \leq 1/2 - \varepsilon, \\ -\dfrac{2\sqrt{\pi}}{B^2}\Theta_0^{\mathrm{p2}}(r) & : k = 0, |h^{-1}r| \leq 1/2 - \varepsilon, \\ K_{\mathrm{B}}(k,r) & : |h^{-1}r| \in (1/2 - \varepsilon, 1/2], \end{cases} \tag{4.11}$$

where we claim that each function $K_{\mathrm{B}}(k,\cdot) : [-h/2 + h\varepsilon, -h/2] \cup [h/2, h/2 - h\varepsilon] \to \mathbb{R}$ fulfills the Hermite interpolation conditions

$$\frac{\partial^j}{\partial r^j} K_{\mathrm{B}}(k, h/2 - h\varepsilon) = \begin{cases} \frac{1}{2B} \frac{\partial^j}{\partial r^j} \Theta^{\mathrm{p2}}(k, h/2 - h\varepsilon) & : k \neq 0 \\ -\frac{2\sqrt{\pi}}{B^2} \frac{\mathrm{d}^j}{\mathrm{d}r^j} \Theta_0^{\mathrm{p2}}(h/2 - h\varepsilon) & : k = 0 \end{cases}, \tag{4.12}$$

$$\frac{\partial^j}{\partial r^j} K_{\mathrm{B}}(k, -h/2 + h\varepsilon) = \begin{cases} \frac{1}{2B} \frac{\partial^j}{\partial r^j} \Theta^{\mathrm{p2}}(k, -h/2 + h\varepsilon) & : k \neq 0 \\ -\frac{2\sqrt{\pi}}{B^2} \frac{\mathrm{d}^j}{\mathrm{d}r^j} \Theta_0^{\mathrm{p2}}(-h/2 + h\varepsilon) & : k = 0 \end{cases} \tag{4.13}$$

for all $j = 0, \ldots, p-1$. Hereby, we refer to $p \in \mathbb{N}$ as the degree of smoothness. In order to end up with h-periodic, smooth functions $K_{\mathrm{R}}(k,\cdot)$, the functions $K_{\mathrm{B}}(k,\cdot)$ are constructed such that

$$\frac{\partial^j}{\partial r^j} K_{\mathrm{R}}(k, h/2) = \frac{\partial^j}{\partial r^j} K_{\mathrm{R}}(k, -h/2), \quad j = 0, \ldots, p-1$$

is also fulfilled. In Section 4.2.2 we show that the functions $K_B(k,.)$ can be constructed as polynomials of degree $2p-1$ by two point Taylor interpolation. Figure 4.1 shows an example of such a regularization $K_{\mathrm{R}}(k,\cdot)$.

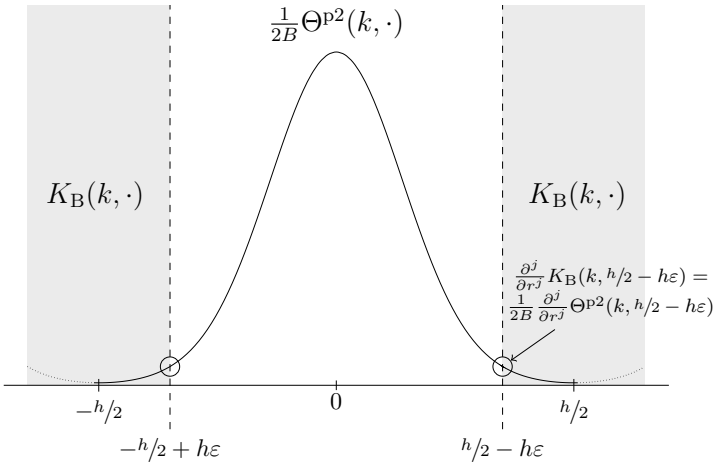

Figure 4.1: Example for $K_{\mathrm{R}}(k,\cdot)$ for $k \geq 1$. At the boundaries (gray area) the regularization adopts the values of the boundary function $K_{\mathrm{B}}(k,\cdot)$. We also marked the points, where the conditions (4.12) and (4.13) are fulfilled.

In summary, the functions $K_{\mathrm{R}}(k,\cdot)$ are h-periodic and smooth, i.e., $K_{\mathrm{R}}(k,\cdot) \in \mathcal{H}^p(h\mathbb{T})$. Therefore, they can be approximated by a truncated Fourier series up to a prescribed error. To this end, we approximate for each $k \in \{\|\boldsymbol{k}\| \neq 0 : \boldsymbol{k} \in \mathcal{I}_{\tilde{\boldsymbol{M}}}\}$ the function

$$\frac{1}{2B} \Theta^{\mathrm{p2}}(k, r) \approx \sum_{l \in \mathcal{I}_{M_3}} \hat{b}_{k,l} \mathrm{e}^{2\pi \mathrm{i} l r / h} \tag{4.14}$$

for $|r| \leq h/2 - h\varepsilon$ by the truncated Fourier series of its regularization $K_{\mathrm{R}}(k,\cdot)$. Analogously, for $k = 0$ we have

$$-\frac{2\sqrt{\pi}}{B^2} \Theta_0^{\mathrm{p2}}(r) \approx \sum_{l \in \mathcal{I}_{M_3}} \hat{b}_{0,l} \mathrm{e}^{2\pi \mathrm{i} l r / h}. \tag{4.15}$$

Thereby, we choose the frequency cutoff $M_3 \in 2\mathbb{N}$ large enough and compute the Fourier coefficients $\hat{b}_{k,l}$ in (4.14) as well as $\hat{b}_{0,l}$ in (4.15) by the discrete Fourier transform

$$\hat{b}_{k,l} := \frac{1}{M_3} \sum_{j \in \mathcal{I}_{M_3}} K_{\mathrm{R}}\left(k, \tfrac{jh}{M_3}\right) \mathrm{e}^{-2\pi \mathrm{i} jl/M_3}, \qquad l = -M_3/2, \dots, M_3/2 - 1. \tag{4.16}$$

This ansatz is closely related to the fast summation method described in [33]. Due to the fact that for each k we have $\Theta^{\mathrm{p2}}(k, \cdot) \in \mathrm{C}^\infty(\mathbb{R})$ we are not restricted in the choice of the parameter p. By choosing M_3 large enough we can construct approximations (4.14) of a required accuracy.

In summary, we obtain the following approximation for the long range parts,

$$\begin{aligned} \phi^{\mathrm{p2,L}}(\boldsymbol{x}_j) + \phi^{\mathrm{p2},\mathbf{0}}(\boldsymbol{x}_j) &\approx \sum_{\boldsymbol{k} \in \mathcal{I}_{\tilde{\boldsymbol{M}}}} \sum_{l \in \mathcal{I}_{M_3}} \hat{b}_{\|\boldsymbol{k}\|,l} \sum_{i=1}^{N} q_i \mathrm{e}^{2\pi \mathrm{i} \boldsymbol{k} \cdot \tilde{\boldsymbol{x}}_{ij}/B} \mathrm{e}^{2\pi \mathrm{i} l x_{ij,3}/h} \\ &= \sum_{(\boldsymbol{k},l) \in \mathcal{I}_{\boldsymbol{M}}} \hat{b}_{\|\boldsymbol{k}\|,l} \left(\sum_{i=1}^{N} q_i \mathrm{e}^{2\pi \mathrm{i} \boldsymbol{v}(\boldsymbol{k},l) \cdot \boldsymbol{x}_i} \right) \mathrm{e}^{-2\pi \mathrm{i} \boldsymbol{v}(\boldsymbol{k},l) \cdot \boldsymbol{x}_j}, \end{aligned} \tag{4.17}$$

where we substitute the truncated Fourier series (4.14), (4.15) into Theorem 4.1 and define $\boldsymbol{M} := (\tilde{\boldsymbol{M}}, M_3) \in 2\mathbb{N}^3$ as well as the vectors $\boldsymbol{v}(\boldsymbol{k}, l) := (\boldsymbol{k}/B, l/h) \in B^{-1}\mathbb{Z}^2 \times h^{-1}\mathbb{Z}$. The expressions in the inner brackets

$$\hat{S}(\boldsymbol{k}, l) := \sum_{i=1}^{N} q_i \mathrm{e}^{2\pi \mathrm{i} \boldsymbol{v}(\boldsymbol{k},l) \cdot \boldsymbol{x}_i}, \quad (\boldsymbol{k}, l) \in \mathcal{I}_{\boldsymbol{M}} \tag{4.18}$$

can be computed by an NFFT$^{\mathrm{H}}$. This will be followed by $|\mathcal{I}_{\boldsymbol{M}}|$ multiplications with $\hat{b}_{\|\boldsymbol{k}\|,l}$ and completed by an NFFT to compute the outer summation with the complex exponentials. Therefore, the proposed evaluation of $\phi^{\mathrm{p2,L}}(\boldsymbol{x}_j) + \phi^{\mathrm{p2},\mathbf{0}}(\boldsymbol{x}_j)$ at the points $\boldsymbol{x}_j$, $j = 1, \dots, N$, requires $\mathcal{O}(N + |\mathcal{I}_{\boldsymbol{M}}| \log |\mathcal{I}_{\boldsymbol{M}}|)$ arithmetic operations.

The calculation of the forces is done analogously to the 3d-periodic case. We set $\mathcal{S} := \mathbb{Z}^2 \times \{0\}$, define $\boldsymbol{F}^{\mathrm{p2}}(\boldsymbol{x}_j) := \boldsymbol{F}_{\mathcal{S}}(\boldsymbol{x}_j)$ via (1.4) and calculate the short range portions $\boldsymbol{F}^{\mathrm{p2,S}}(\boldsymbol{x}_j)$ given by (3.5) via a direct summation. In the long range part we can either use the i$\boldsymbol{k}$ approach, i.e., we set

$$\boldsymbol{F}^{\mathrm{p2,L}}(\boldsymbol{x}_j) + \boldsymbol{F}^{\mathrm{p2},\mathbf{0}}(\boldsymbol{x}_j) \approx 2\pi \mathrm{i} q_j \sum_{(\boldsymbol{k},l) \in \mathcal{I}_{\boldsymbol{M}}} \hat{b}_{\|\boldsymbol{k}\|,l} \left(\sum_{i=1}^{N} q_i \mathrm{e}^{2\pi \mathrm{i} \boldsymbol{v}(\boldsymbol{k},l) \cdot \boldsymbol{x}_i} \right) \boldsymbol{v}(\boldsymbol{k}, l) \mathrm{e}^{-2\pi \mathrm{i} \boldsymbol{v}(\boldsymbol{k},l) \cdot \boldsymbol{x}_j}, \tag{4.19}$$

or the analytic differentiation, where the ∇ operator is applied to the window function $\tilde{\varphi}$ in (2.3) within the NFFT, cf. (3.6).

In summary, we obtain Algorithm 4.3 for the fast computation of 2d-periodic Coulomb interactions.

Algorithm 4.3 (2d-periodic P^{2}NFFT)**.**

Input: Positions $\boldsymbol{x}_j \in B\mathbb{T}^2 \times [-B_3/2, B_3/2]$, charges $q_j \in \mathbb{R}$ $(j = 1, \dots, N)$, splitting parameter $\alpha > 0$, short range cutoff $r_{\mathrm{cut}} > 0$, long range cutoff $\boldsymbol{M} = (\tilde{\boldsymbol{M}}, M_3) \in 2\mathbb{N}^3$, regularization parameter $\varepsilon > 0$, degree of smoothness $p \in \mathbb{N}$.

0.) Precomputations:
   a) Set $h := (1/2 - \varepsilon)^{-1} B_3$.
   b) Construct the regularization (4.11) for each $k \in \{\|\boldsymbol{k}\| : \boldsymbol{k} \in \mathcal{I}_{\tilde{M}}\}$.
   c) Compute the Fourier coefficients (4.16).

1.) Compute the short range parts of the potentials $\phi^{\mathrm{p2,S}}(\boldsymbol{x}_j)$ and the short range parts of the forces $\boldsymbol{F}^{\mathrm{p2,S}}(\boldsymbol{x}_j)$ by direct evaluation, i.e., restrict the summation in (4.3) and (3.5), where $\mathcal{S} := \mathbb{Z}^2 \times \{0\}$, to all $\|\boldsymbol{x}_{ij} + B\boldsymbol{n}\| \leq r_{\mathrm{cut}}$.

2.) Compute the sums $\hat{S}(\boldsymbol{k}, l)$ in (4.18) by the adjoint NFFT (2.4).

3.) Apply the NFFT (2.2) to compute the long range parts of the potentials $\phi^{\mathrm{p2,L}}(\boldsymbol{x}_j) + \phi^{\mathrm{p2},\mathbf{0}}(\boldsymbol{x}_j)$ by (4.17).

4.) Compute the long range parts of the forces $\boldsymbol{F}^{\mathrm{p2,L}}(\boldsymbol{x}_j) + \boldsymbol{F}^{\mathrm{p2},\mathbf{0}}(\boldsymbol{x}_j)$ via the i$\boldsymbol{k}$ differentiation approach (4.19) or the analytic differentiation, cf. (3.6).

5.) For all $j = 1, \ldots, N$ compute

$$\begin{aligned}\phi^{\mathrm{p2}}(\boldsymbol{x}_j) &= \phi^{\mathrm{p2,S}}(\boldsymbol{x}_j) + \phi^{\mathrm{p2,L}}(\boldsymbol{x}_j) + \phi^{\mathrm{p2},\mathbf{0}}(\boldsymbol{x}_j) + \phi^{\mathrm{p2,self}}(\boldsymbol{x}_j)\\ \boldsymbol{F}^{\mathrm{p2}}(\boldsymbol{x}_j) &= \boldsymbol{F}^{\mathrm{p2,S}}(\boldsymbol{x}_j) + \boldsymbol{F}^{\mathrm{p2,L}}(\boldsymbol{x}_j) + \boldsymbol{F}^{\mathrm{p2},\mathbf{0}}(\boldsymbol{x}_j).\end{aligned}$$

6.) Compute the energy (4.2).

Output: Energy U^{p2}, potentials $\phi^{\mathrm{p2}}(\boldsymbol{x}_j)$ and forces $\boldsymbol{F}^{\mathrm{p2}}(\boldsymbol{x}_j)$.

Remark 4.4. Algorithm 4.3 has the same structure as the NFFT based method for 3d-periodic systems, cf. Section 3. Thus, we also obtain a matrix vector notation of the form (3.4) for the approximation of $\phi^{\mathrm{p2,L}}(\boldsymbol{x}_j) + \phi^{\mathrm{p2},\mathbf{0}}(\boldsymbol{x}_j)$. In other words, we use the same algorithm, where we replace the Fourier coefficients $\hat{b}_{\boldsymbol{k}}$ from (3.3) by the new coefficients $\hat{b}_{\boldsymbol{k},l}$ in (4.16) and insert the nodes $(\tilde{\boldsymbol{x}}_{ij}/B, x_{ij,3}/h) \in \mathbb{T}^3$ instead of $\boldsymbol{x}_{ij}/B \in \mathbb{T}^3$ into the NFFT algorithms. □

4.2.2. Implementation details

The precomputation step of Algorithm 4.3 includes the construction of the regularizations (4.11). Thereby, we obtain $K_{\mathrm{B}}(k, \cdot)$ by the unique polynomial of degree $2p-1$ that fulfills the $2p$ Hermite interpolation conditions (4.12) – (4.13) in two points. An explicit representation of this polynomial is given by Theorem A.1 in the appendix, where we set $m = h/2$ and $r = h\varepsilon$ and a_j, b_j equal to the right hand sides of the interpolation conditions (4.12) – (4.13), respectively.

In order to compute the derivatives in (4.12) – (4.13) we use the following relations. We define the function

$$\Theta_1(k, r) := \mathrm{e}^{2\pi k r/B} \mathrm{erfc}\left(\frac{\pi k}{\alpha B} + \alpha r\right) \tag{4.20}$$

and let $\Theta_{\pm}(k, r) := \Theta_1(k, r) \pm \Theta_1(k, -r)$. Note that we have $\Theta^{\mathrm{p2}}(k, r) = \frac{1}{k}\Theta_+(k, r)$. We immediately see that

$$\begin{aligned}\frac{\partial}{\partial r}\Theta_+(k, r) &= \frac{2\pi k}{B}\Theta_-(k, r),\\ \frac{\partial}{\partial r}\Theta_-(k, r) &= \frac{2\pi k}{B}\Theta_+(k, r) - \frac{4\alpha}{\sqrt{\pi}}\mathrm{e}^{-\alpha^2 r^2 - \pi^2 k^2/\alpha^2 B^2},\end{aligned}$$

and, therefore,

$$\frac{\partial^2}{\partial r^2}\Theta_+(k,r) = \frac{4\pi^2k^2}{B^2}\Theta_+(k,r) - \frac{8\alpha\sqrt{\pi}k}{B}\mathrm{e}^{-\alpha^2r^2-\pi^2k^2/\alpha^2B^2}.$$

For the computation of the derivatives of order $n \geq 2$ we use the following recursive formula

$$\frac{\partial^n}{\partial r^n}\Theta_+(k,r) = \frac{4\pi^2k^2}{B^2}\frac{\partial^{(n-2)}}{\partial r^{(n-2)}}\Theta_+(k,r) - \frac{\partial^{(n-2)}}{\partial r^{(n-2)}}\frac{8\alpha\sqrt{\pi}k}{B}\mathrm{e}^{-\alpha^2r^2-\pi^2k^2/\alpha^2B^2}.$$

The second term can be computed easily with the derivatives of the Gaussian window function

$$\frac{\partial^{(n-2)}}{\partial r^{(n-2)}}\frac{8\alpha\sqrt{\pi}k}{B}\mathrm{e}^{-\alpha^2r^2-\pi^2k^2/\alpha^2B^2} = \frac{8\alpha\sqrt{\pi}k}{B}\mathrm{e}^{-\pi^2k^2/\alpha^2B^2}\frac{\partial^{(n-2)}}{\partial r^{(n-2)}}\mathrm{e}^{-\alpha^2r^2}.$$

We remark that the numerical evaluation of the function (4.20) for large $k, r > 0$ is important in order to obtain a regularization of the 2d-periodic Ewald splitting. This can be done straight forward for $r \leq 0$, since we have the trivial upper bound $\Theta_1(k,r) \leq 2$. In contrast, for large values of $r > 0$ the exponential tends to infinity and exceeds rapidly the range of representable floating point numbers in double precision. Since the complementary error function tends much faster to zero, the function $\Theta(k,r)$ can be considered numerically equal to zero for $kr > 0$ large enough. For the substitutions $l = \frac{\pi k}{B\alpha} > 0$ and $t = lr\alpha > 0$ we can use the standard estimate $0 \leq (l - \sqrt{t})^2$ that yields $2\sqrt{t} \leq l + t/l$ and, finally, we obtain

$$\Theta_1\left(\frac{lB\alpha}{\pi}, \frac{tB}{\pi k}\right) = \mathrm{e}^{2t}\mathrm{erfc}\left(l + \tfrac{t}{l}\right) \leq \mathrm{e}^{2t}\mathrm{erfc}\left(2\sqrt{t}\right) =: f(t).$$

The right hand side holds $f(t) \leq 10^{-16}$ for $t > 18$, i.e., whenever $t := \frac{\pi kr}{B} > 18$ we can assume $\Theta_1(k,r)$ to be numerically equal to zero.

4.3. Numerical results

In this section we present numerical results of our algorithm for 2d-periodic boundary conditions. We implemented this algorithm as a part of the P^{2}NFFT solver [31] within the Scalable Fast Coulomb Solver (ScaFaCoS) library [1], i.e., our implementation is publicly available at [1] and can be compared to various other well established methods with respect to accuracy and run time. Recently, this library has been used for a broad comparison of various fast Coulomb solvers for fully 3d-periodic boundary conditions [5]. In the following, we show that our 2d-periodic algorithm can be tuned to high accuracy and offers a run time comparable to the well established P^{3}M algorithm for 3d-periodic systems.

For all tests the calculation of the forces was performed using the analytic differentiation approach, cf. (3.6). Whenever the rms field error is examined, the comparative data were computed with the fast multipole method [11, 23, 22] within ScaFaCoS tuned to sufficient accuracy.

Our run time measurements have been performed on an Intel i5-2400 single core processor that runs on 3.10 GHz with 8 GB main memory. The software was built with the GCC C compiler at version 4.7.1 and optimization flags "-O3".

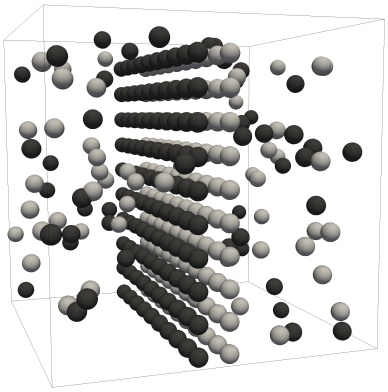

Figure 4.2: Cloud wall system with $N = 300$ charges $q_j = \pm 1$ in a cubic box, see [5].

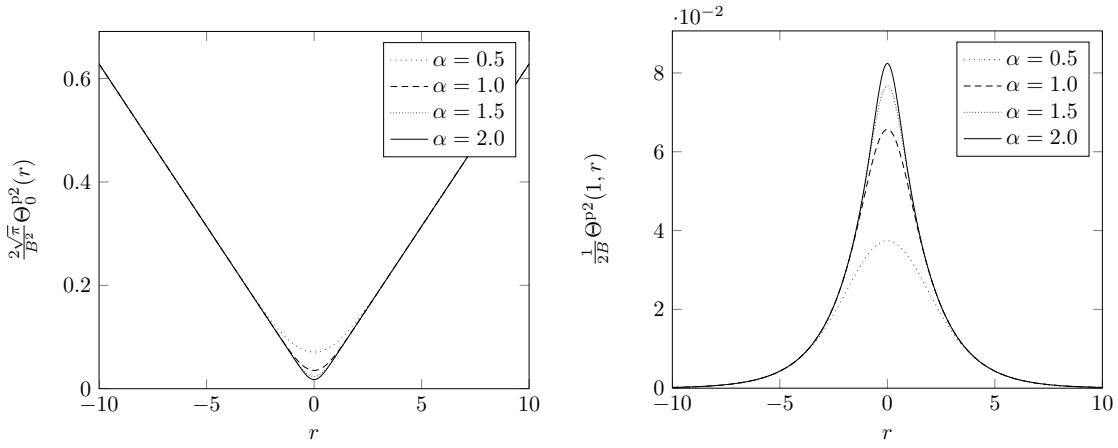

Figure 4.3: $\Theta_0^{\mathrm{p2}}(r)$ and $\Theta^{\mathrm{p2}}(1, r)$ with $B = 10$ for different splitting parameters α.

Example 4.5. We consider a so called cloud wall system consisting of $N = 300$ charges in a cubic box of edge length $B = 10$ (see Figure 4.2). The system consists of a diffusive particle cloud surrounding two oppositely charged walls and was proposed in [5] because of its significant long range part.

In order to get an impression of the involved functions in (4.11) we plot these functions over the interval $[-B, B]$ for different values of α, see Figure 4.3.

In the following we choose the degree of smoothness $p = 6$, set $M_3 = 64$ and investigate the exactness of (4.15) as well as of (4.14) for $k = 1$ and $k = 3$ in dependency on the parameter ε in (4.11). Therefore, we plot the maximum approximation errors in Figure 4.4, where the maximum error of (4.15) is depicted in black. It can be seen that, for some fixed ε, the errors decrease as $\alpha \to 0$. On the other hand, the value of the optimal ε increases as $\alpha \to 0$. Additionally, we plot the error in the case $k = 1$ (blue) and for $k = 3$ (red).

In Figure 4.5 we choose the same values for ε and plot the relative rms field error (1.7) in the cloud wall system as a function of the splitting parameter α, where we choose $\boldsymbol{M} = (64, 64, 64)$ and $\boldsymbol{m} = (64, 64, 128)$ in (2.3). It can be seen that for ε too small we obtain a plateau in the error plot, i.e., the error remains almost constant over a certain interval. If ε is chosen large enough, the optimal approximation error becomes smaller, whereas for large values of α the

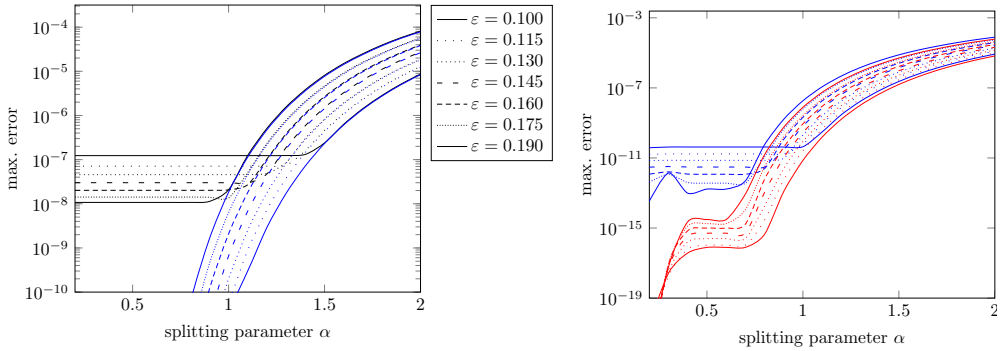

Figure 4.4: Approximation errors for different values of ε with $M_3 = 64$ and $p = 6$.
left: Maximum errors of (4.15) (black) and of (4.14) for $k = 1$ (blue).
right: Maximum errors of (4.14) for $k = 1$ (blue) as well as for $k = 3$ (red).

error is even worse. We obtain the smallest error for $\varepsilon \approx 0.145$, where the optimal $\alpha \approx 1$, which kind of goes along with the results plotted in Figure 4.4.

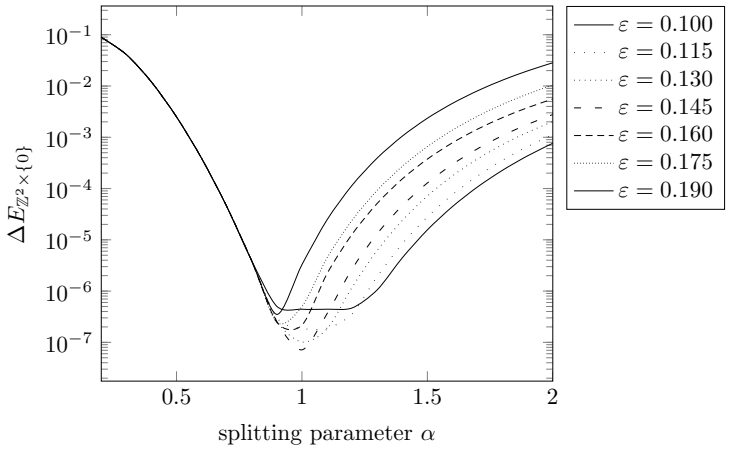

Figure 4.5: Relative rms field error (1.7) over α for different regularization parameters ε. We choose the short rang cutoff $r_{\text{cut}} = 4$, the smoothness $p = 6$, $\boldsymbol{M} = (64, 64, 64)$, $\boldsymbol{m} = (64, 64, 128)$ and the B-Spline of order 8 as NFFT window function φ in Algorithm 4.3.

Obviously, the value of the optimal ε depends on both, the exactness of the approximation of Θ_0^{p2} in the $k = 0$ part as well as the goodness of the approximations of the kernel functions for $k > 0$, but the error is dominated by the approximation in the $k = 0$ part.

In Figure 4.6 we plot the relative rms field error $\triangle E_{\mathbb{Z}^2\times\{0\}}$ with respect to the splitting parameter α for different FFT sizes $\boldsymbol{M} = (M, M, M)$. In the case $M = 64$ we set $\varepsilon := 0.145$. For the other values of M we tuned ε by hand in order to get a small optimal rms field error. On the right hand side we see the corresponding errors of the same particle system treated under fully periodic boundary conditions. Of course, the 2d-periodic calculation produces larger errors in the long range calculations, which is due to the fact that each approximation (4.14) generates a certain error, whereas in the 3d-periodic case the Fourier

coefficients (3.3) are exactly known. As the errors in the short range part behave exactly the same way, the splitting parameter α adopts slightly different optimal values.

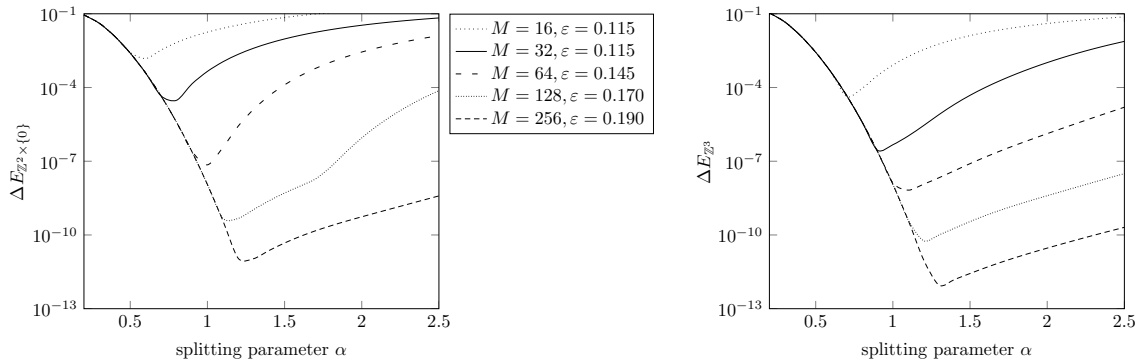

Figure 4.6: The relative rms field error (1.7) over α for different FFT sizes. We choose the short range cutoff $r_{\text{cut}} = 4$, the smoothness $p = 6$, $\boldsymbol{m} = (M, M, 2M)$ and the B-Spline of order 8 as NFFT window function φ in Algorithm 4.3. We plot the results of the 2d-periodic (left) as well as of the 3d-periodic computation (right).

□

Example 4.6. We compute the potentials $\phi^{\text{p2}}(\boldsymbol{x}_j)$ as well as the forces $F^{\text{p2}}(\boldsymbol{x}_j)$ in cloud wall systems of different size, where the particles are distributed in a cubic box of edge length B.

It can be seen from the data in Table 4.1 that the systems have the same particle density. Therefore, the computations in the near field with fixed values of the short range cutoff r_{cut} and the splitting parameter α are comparable. In the calculation for the long range part we choose $\boldsymbol{M} = (M, M, M) \in 2\mathbb{N}^3$ in (4.17) and apply the NFFT with oversampling factor 2 regarding the nonperiodic dimension, i.e., we set $\boldsymbol{m} := (M, M, 2M)$ in the NFFT approximation (2.3) . In addition, we do the same calculation without oversampling, where we set $\boldsymbol{m} := (M, M, M)$, and treat the same particle system under fully periodic boundary conditions. As a window function we choose the cardinal B-spline of order 8 and construct regularizations of smoothness $p = 6$. Note that in the case without oversampling the choice of the parameters is the same as for the P^{3}M.

For the cloud wall system of size $N = 300$ we set $M = 16$ and $\varepsilon = 0.115$ as in the last example. For the short range cutoff $r_{\text{cut}} = 4$ we find from Figure 4.6 that the error $\triangle E_{\mathbb{Z}^2\times\{0\}}$ is minimized for $\alpha \approx 0.6$. For the larger systems we choose larger values of M. Consequently, we also have to choose other values for ε, too. For this reason we consider the error of the approximation (4.15) for the different combinations of B and M, where we fix the splitting parameter $\alpha = 0.6$, see Figure 4.7.

For $M = 16$ we obtain the optimal value $\varepsilon_{\text{opt}} \approx 0.13$ regarding the exactness (4.15), whereas we obtain the minimal rms field error $\triangle E_{\mathbb{Z}^2\times\{0\}}$ for $\varepsilon \approx 0.115 \approx 0.8846 \cdot 0.13$. Therefore, we heuristically set $\varepsilon = 0.8846 \cdot \varepsilon_{\text{opt}}$ also in the other cases.

In Table 4.1 it can be seen that we achieve approximation errors of comparable size among all systems. The fact that we are not far away from the errors of the 3d-periodic calculation shows that the parameters where chosen appropriately.

In Figure 4.8 we plot the corresponding run times. We see that the oversampling slightly increases the run time and that the fully periodic as well as the 2d-periodic calculation

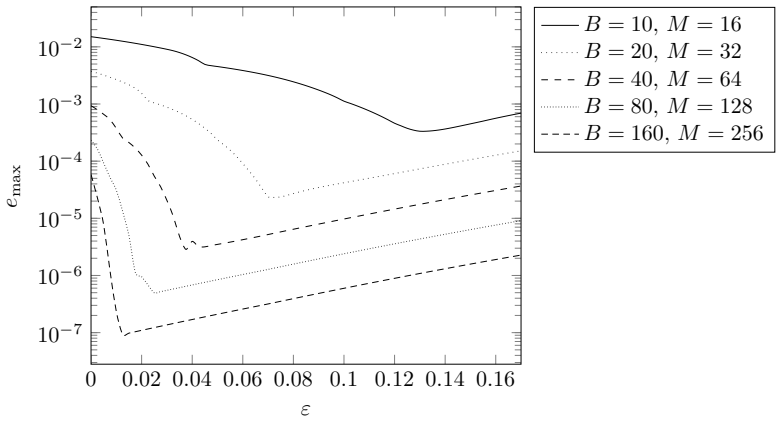

Figure 4.7: Maximum approximation error (4.15) for $k = 0$ over ε, where we choose the splitting parameter $\alpha = 0.6$.

N	B	ε	M	oversampling $\Delta E_{\mathbb{Z}^2\times\{0\}}$	no oversampling $\Delta E_{\mathbb{Z}^2\times\{0\}}$	$\Delta E_{\mathbb{Z}^3}$
300	10	0.1150	16	1.5118e-03	4.3565e-03	4.1514e-04
2400	20	0.0641	32	7.6972e-04	1.1836e-03	4.1514e-04
19200	40	0.0332	64	5.5538e-04	8.2526e-04	4.1514e-04
153600	80	0.0221	128	5.2104e-04	7.6865e-04	4.1514e-04
1228800	160	0.0111	256	5.1955e-04	8.0417e-04	4.1514e-04

Table 4.1: Relative rms force errors in the cloud wall systems under 2d-periodic boundary conditions (with and without oversampling in the third dimension) as well as under fully periodic boundary conditions. These errors have been obtained with short range cutoff $r_{\text{cut}} = 4$ and splitting parameter $\alpha = 0.6$.

without oversampling require almost the same amount of time. In summary, we remark that in contrast to the fully periodic case, where the Fourier coefficients are given analytically by (3.3), we have to precompute all the coefficients $\hat{b}_{\boldsymbol{k},l}$ in (4.16). Of course, this leads to a huge amount of precomputation steps for large values of M, which is not included in the stated run times. However, if one is interested in doing a large simulation with fixed parameters, the precomputations have to be done only once. □

5. Fast Ewald summation for 1d-periodic boundary conditions

5.1. Ewald summation

We consider a system of N charges $q_j \in \mathbb{R}$ at positions $\boldsymbol{x}_j \in B\mathbb{T} \times \mathbb{R}^2$. If periodic boundary conditions are assumed only in the first coordinate we define the potential of each single particle j by

$$\phi^{\mathrm{p1}}(\boldsymbol{x}_j) := \phi_{\mathbb{Z}\times\{0\}^2}(\boldsymbol{x}_j) = \sum_{s=0}^{\infty} \sum_{\substack{\boldsymbol{n}\in\mathbb{Z}\times\{0\}^2 \\ |n_1|=s}} {\sum_{i=1}^{N}}' \frac{q_i}{\|\boldsymbol{x}_{ij} + B\boldsymbol{n}\|} \tag{5.1}$$

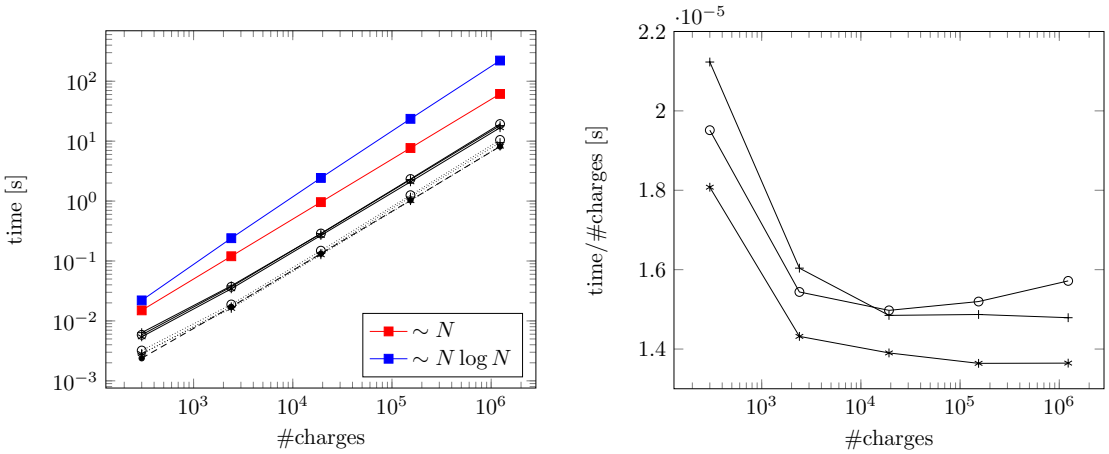

Figure 4.8: Computation times with oversampling (o) and without oversampling (∗) for the 2d-periodic case as well as for the fully periodic computation (+).
left: Attended times for the total computation (solid lines), the long range part (dotted) as well as the short range part (dashed). We also plot exemplary behaviors where the run time grows proportional to N (red) and $N \log N$ (blue).
right: Total computation time scaled by the number of particles.
We achieved rms field errors of the size $\approx 5 \cdot 10^{-4}$.

and define the Coulomb energy

$$U^{\mathrm{p1}} := U_{\mathbb{Z}\times\{0\}^2} = \frac{1}{2}\sum_{j=1}^{N} q_j \phi^{\mathrm{p1}}(\boldsymbol{x}_j),$$

i.e., we set $\mathcal{S} := \mathbb{Z}\times\{0\}^2$ in (1.2) – (1.4) and consider the spherical limit analogously to (3.1). In this section we denote for some $\boldsymbol{y} = (y_1, y_2, y_3) \in \mathbb{R}^3$ the vector of its last two components by $\tilde{\boldsymbol{y}} := (y_2, y_3) \in \mathbb{R}^2$.

The result of the following Lemma will be used in the derivation of the Ewald formulas.

Lemma 5.1. *For $\beta > 0$ and $n \in \mathbb{N}$ we have*

$$\int_0^\beta \frac{x^{2n}\mathrm{d}x}{\sqrt{1+x^2}} = (-1)^n \frac{(2n-1)!!}{(2n)!!}\left(\sqrt{1+\beta^2}\sum_{k=1}^{n}(-1)^k\frac{(2k-2)!!}{(2k-1)!!}\beta^{2k-1} + \ln(\beta+\sqrt{1+\beta^2})\right).$$

Proof. In the case $n = 0$ we obtain

$$\int_0^\beta \frac{\mathrm{d}x}{\sqrt{1+x^2}} = \operatorname{arsinh}(\beta) = \ln(\beta+\sqrt{1+\beta^2}).$$

For $n \in \mathbb{N}$ we get

$$\begin{aligned}\int_0^\beta \frac{x^{2n}\mathrm{d}x}{\sqrt{1+x^2}} = \int_0^\beta x^{2n-1}\frac{x\mathrm{d}x}{\sqrt{1+x^2}} &= \beta^{2n-1}\sqrt{1+\beta^2} - (2n-1)\int_0^\beta x^{2n-2}\sqrt{1+x^2}\mathrm{d}x \\ &= \beta^{2n-1}\sqrt{1+\beta^2} - (2n-1)\int_0^\beta x^{2n-2}\frac{1+x^2}{\sqrt{1+x^2}}\mathrm{d}x \\ \iff \int_0^\beta \frac{x^{2n}\mathrm{d}x}{\sqrt{1+x^2}} &= \frac{1}{2n}\left(\beta^{2n-1}\sqrt{1+\beta^2} - (2n-1)\int_0^\beta \frac{x^{2n-2}}{\sqrt{1+x^2}}\mathrm{d}x\right)\end{aligned}$$

and the claim follows by induction. ∎

In the following we denote by

$$\Gamma(s,x) := \int_x^\infty t^{s-1}\mathrm{e}^{-t}\mathrm{d}t \tag{5.2}$$

the upper incomplete gamma function. For the case $s = 0$ the well known identity

$$\Gamma(0,x) = -\gamma - \ln x - \sum_{k=1}^{\infty}(-1)^k \frac{x^k}{k!k} \tag{5.3}$$

holds for all positive x, see [2, number 5.1.11]. Thereby, γ is the Euler-Mascheroni constant. The function $\Gamma(0,\cdot)$ is also known as the exponential integral function. We easily see

$$\lim_{x\to 0} \Gamma(0,x) + \ln x + \gamma = 0. \tag{5.4}$$

In the following Theorem, we consider the 1d-Ewald formula, see [32], and give a proof using convergence factors, analogously to the proof of Theorem 4.1.

Theorem 5.2. *Consider an electrical neutral system of N charges $q_j \in \mathbb{R}$ at positions $\boldsymbol{x}_j = (x_{j,1}, \tilde{\boldsymbol{x}}_j) \in B\mathbb{T}\times\mathbb{R}^2$, $j = 1,\dots,N$. Under periodic boundary conditions in the first variable the potential $\phi^{\mathrm{p1}}(\boldsymbol{x}_j)$, defined in (5.1), can be written as*

$$\phi^{\mathrm{p1}}(\boldsymbol{x}_j) = \phi^{\mathrm{p1,S}}(\boldsymbol{x}_j) + \phi^{\mathrm{p1,L}}(\boldsymbol{x}_j) + \phi^{\mathrm{p1,0}}(\boldsymbol{x}_j) + \phi^{\mathrm{p1,self}}(\boldsymbol{x}_j),$$

where for the splitting parameter $\alpha > 0$ we define the short range part

$$\phi^{\mathrm{p1,S}}(\boldsymbol{x}_j) := \sum_{\boldsymbol{n}\in\mathbb{Z}\times\{0\}^2} {\sum_{i=1}^{N}}' q_i \frac{\mathrm{erfc}(\alpha\|\boldsymbol{x}_{ij} + B\boldsymbol{n}\|)}{\|\boldsymbol{x}_{ij} + B\boldsymbol{n}\|}, \tag{5.5}$$

the long range parts

$$\phi^{\mathrm{p1,L}}(\boldsymbol{x}_j) := \frac{2}{B}\sum_{k\in\mathbb{Z}\setminus\{0\}}\sum_{i=1}^{N} q_i\, \mathrm{e}^{2\pi i k(x_{i,1}-x_{j,1})/B}\cdot\Theta^{\mathrm{p1}}(k,\|\tilde{\boldsymbol{x}}_{ij}\|)$$

$$\phi^{\mathrm{p1,0}}(\boldsymbol{x}_j) := -\frac{1}{B}\sum_{\substack{i=1\\ \|\tilde{\boldsymbol{x}}_{ij}\|\neq 0}}^{N} q_i\left[\gamma + \Gamma(0,\alpha^2\|\tilde{\boldsymbol{x}}_{ij}\|^2) + \ln(\alpha^2\|\tilde{\boldsymbol{x}}_{ij}\|^2)\right],$$

the self potential

$$\phi^{\mathrm{p1,self}}(\boldsymbol{x}_j) := -\frac{2\alpha}{\sqrt{\pi}} q_j\ ,$$

and the function $\Theta^{\mathrm{p1}}(k,r)$ for $k, r \in \mathbb{R}$ is defined by

$$\Theta^{\mathrm{p1}}(k,r) = \int_0^\alpha \frac{1}{z}\mathrm{e}^{\frac{-\pi^2k^2}{B^2z^2}}\mathrm{e}^{-r^2z^2}\mathrm{d}z\,. \tag{5.6}$$

Proof. As in Theorem 4.1 we apply the convergence factor $\mathrm{e}^{-s\|\boldsymbol{x}_{ij}+B\boldsymbol{n}\|^2}$ for the calculation of the potential (5.1). After using the splitting (1.5) we obtain

$$\phi^{\mathrm{p1}}(\boldsymbol{x}_j) = \phi^{\mathrm{p1,S}}(\boldsymbol{x}_j) + \sum_{\boldsymbol{n}\in\mathbb{Z}\times\{0\}^2} \sum_{i=1}^{N} q_i \frac{\operatorname{erf}(\alpha\|\boldsymbol{x}_{ij}+B\boldsymbol{n}\|)}{\|\boldsymbol{x}_{ij}+B\boldsymbol{n}\|} + \phi^{\mathrm{p1,self}}(\boldsymbol{x}_j).$$

We define

$$\phi_s(\boldsymbol{x}_j) := \sum_{\boldsymbol{n}\in\mathbb{Z}\times\{0\}^2} \sum_{i=1}^{N} q_i \mathrm{e}^{-s\|\boldsymbol{x}_{ij}+B\boldsymbol{n}\|^2} \frac{\operatorname{erf}(\alpha\|\boldsymbol{x}_{ij}+B\boldsymbol{n}\|)}{\|\boldsymbol{x}_{ij}+B\boldsymbol{n}\|}$$

and use the Poisson summation formula

$$\sum_{n\in\mathbb{Z}} \mathrm{e}^{-\beta(x+nB)^2} = \frac{1}{B}\sum_{k\in\mathbb{Z}} \sqrt{\frac{\pi}{\beta}} \mathrm{e}^{-\pi^2k^2/(B^2\beta)} \mathrm{e}^{2\pi\mathrm{i}kx/B}$$

to obtain

$$\phi_s(\boldsymbol{x}_j) = \frac{2}{\sqrt{\pi}} \sum_{k\in\mathbb{Z}} \sum_{i=1}^{N} q_i \frac{\sqrt{\pi}}{B} \mathrm{e}^{2\pi\mathrm{i}k(x_{i,1}-x_{j,1})/B} \int_0^\alpha \frac{1}{\sqrt{s+z^2}} \mathrm{e}^{\frac{-\pi^2k^2}{B^2(s+z^2)}} \mathrm{e}^{-\|\tilde{\boldsymbol{x}}_{ij}\|^2(s+z^2)} \mathrm{d}z,$$

analogously to (4.6). Again, for $k \neq 0$ we compute the limit for $s \to 0$ under the integrals and obtain by similar steps as in the proof of Theorem 4.1

$$\lim_{s\to 0} \phi_s(\boldsymbol{x}_j) = \phi^{\mathrm{p1,L}}(\boldsymbol{x}_j) + \lim_{s\to 0} \frac{2}{B} \sum_{i=1}^{N} q_i \mathrm{e}^{-s\xi_{ij}^2} \int_0^\alpha \frac{\mathrm{e}^{-\xi_{ij}^2 z^2}}{\sqrt{s+z^2}} \mathrm{d}z,$$

where we set $\xi_{ij} := \|\tilde{\boldsymbol{x}}_{ij}\|$. In order to compute the remaining limit for $k = 0$ we make use of the substitution $y := \frac{z}{\sqrt{s}}$ again and get

$$I(s) := \int_0^\alpha \frac{\mathrm{e}^{-\xi_{ij}^2 z^2}}{\sqrt{s+z^2}} \mathrm{d}z = \int_0^{\frac{\alpha}{\sqrt{s}}} \frac{\mathrm{e}^{-s\xi_{ij}^2 z^2}}{\sqrt{1+z^2}} \mathrm{d}z.$$

Replacing the exponential by its Taylor representation in s we have

$$I(s) = \sum_{n=0}^{\infty} \frac{(-1)^n \xi_{ij}^{2n} s^n}{n!} \int_0^{\frac{\alpha}{\sqrt{s}}} \frac{z^{2n}}{\sqrt{1+z^2}} \mathrm{d}z.$$

With the help of Lemma 5.1 we get

$$\int_0^{\frac{\alpha}{\sqrt{s}}} \frac{1}{\sqrt{1+z^2}} \mathrm{d}z = \ln\left(\frac{\alpha}{\sqrt{s}} + \frac{\sqrt{s+\alpha^2}}{\sqrt{s}}\right)$$

for $n = 0$ and in the case $n > 0$ we obtain

$$\begin{aligned} s^n \int_0^{\frac{\alpha}{\sqrt{s}}} \frac{z^{2n}}{\sqrt{1+z^2}} \mathrm{d}z &= (-1)^n \frac{\sqrt{s+\alpha^2}}{\sqrt{s}} s^n \frac{(2n-1)!!}{(2n)!!} \sum_{k=1}^{n} (-1)^k \frac{(2k-2)!!}{(2k-1)!!} \frac{\alpha^{2k-1}\sqrt{s}}{s^k} \\ &\quad + (-1)^n s^n \frac{(2n-1)!!}{(2n)!!} \ln\left(\frac{\alpha}{\sqrt{s}} + \frac{\sqrt{s+\alpha^2}}{\sqrt{s}}\right) \\ &= \mathcal{O}(s) + \sqrt{s+\alpha^2} \cdot \frac{\alpha^{2n-1}}{2n} + (-1)^n s^n \frac{(2n-1)!!}{(2n)!!} \ln\left(\frac{\alpha}{\sqrt{s}} + \frac{\sqrt{s+\alpha^2}}{\sqrt{s}}\right) \end{aligned}$$

for $s \to 0$. Applying (5.3), (5.4) as well as the charge neutrality condition (1.1) we get

$$\begin{aligned}\lim_{s\to 0} \phi_s(\boldsymbol{x}_j) &= \phi^{\mathrm{p1,L}}(\boldsymbol{x}_j) + \lim_{s\to 0} \frac{2}{B} \sum_{i=1}^{N} q_i \mathrm{e}^{-s\xi_{ij}^2} I(s), \\ &= \phi^{\mathrm{p1,L}}(\boldsymbol{x}_j) + \frac{2}{B} \sum_{i=1}^{N} q_i \sum_{n=1}^{\infty} \frac{(-1)^n \xi_{ij}^{2n} \alpha^{2n}}{n! 2n} \\ &= \phi^{\mathrm{p1,L}}(\boldsymbol{x}_j) - \frac{1}{B} \sum_{\substack{i=1 \\ \|\tilde{\boldsymbol{x}}_{ij}\| \neq 0}}^{N} q_i \left[\gamma + \Gamma(0, \alpha^2 \|\tilde{\boldsymbol{x}}_{ij}\|^2) + \ln(\alpha^2 \|\tilde{\boldsymbol{x}}_{ij}\|^2)\right].\end{aligned}$$

■

The function $\Theta^{\mathrm{p1}}(k, r)$ can be expressed by the incomplete modified Bessel function of the second kind [19], see Section 5.2.2. This function is known to be infinitely continuously differentiable and, thus, we can construct regularizations of similar structure as (4.11) in order to construct a fast algorithm. In this case the final algorithm requires a smooth bivariate regularization, which can be obtained easily from a one dimensional construction as the Fourier coefficients are radial in $\tilde{\boldsymbol{x}}_{ij}$. Then, the evaluation is done with the multivariate fast summation method [34].

By the following Lemma 5.3 we show that the function $\Theta^{\mathrm{p1}}(k, r)$ for fixed r tends to zero exponentially fast for growing k, which allows the truncation of the infinite sum in $\phi^{\mathrm{p1,L}}(\boldsymbol{x}_j)$. Furthermore, Lemma 5.4 shows that also the kernel in $\phi^{\mathrm{p1,0}}(\boldsymbol{x}_j)$ is a smooth function, which allows the application of the fast summation method.

Lemma 5.3. *For arbitrary $r \in \mathbb{R}$ we have for the function Θ^{p1} given in* (5.6)

$$\Theta^{\mathrm{p1}}(k, r) \to 0 \text{ with } \Theta^{\mathrm{p1}}(k, r) = o(k^{-2}\mathrm{e}^{-k^2}) \text{ for } k \to \infty.$$

Proof. By the definition (5.6) we immediately see

$$\Theta^{\mathrm{p1}}(k, r) \leq \Theta^{\mathrm{p1}}(k, 0) = \frac{1}{2}\Gamma\left(0, \frac{\pi^2 k^2}{\alpha^2 B^2}\right).$$

The claim follows by applying the asymptotic expansion $\Gamma(0, x) \approx \frac{\mathrm{e}^{-x}}{x}$, cf. [2, number 6.5.32], which holds for large $x := \frac{\pi^2 k^2}{\alpha^2 B^2}$. ■

Lemma 5.4. *For the univariate function*

$$\vartheta(x) := \begin{cases} 0 & : x = 0, \\ \Gamma(0, x^2) + \ln(x^2) + \gamma & : \textit{else} \end{cases}$$

we have $\vartheta \in \mathrm{C}^\infty(\mathbb{R})$.

Proof. Since $\lim_{t\to 0} \Gamma(0, t) + \ln(t) + \gamma = 0$ the function is continuous. As (5.3) holds for all $x > 0$ we obtain

$$\gamma + \Gamma(0, x^2) + \ln(x^2) = \sum_{k=1}^{\infty} \frac{(-1)^{k+1} x^{2k}}{k! k}, \quad x \neq 0.$$

From this representation we easily conclude

$$\lim_{x\to +0} \frac{\mathrm{d}^n}{\mathrm{d}x^n} \left(\gamma + \Gamma(0, x^2) + \ln(x^2)\right) = \lim_{x\to -0} \frac{\mathrm{d}^n}{\mathrm{d}x^n} \left(\gamma + \Gamma(0, x^2) + \ln(x^2)\right) \neq \pm\infty.$$

■

5.2. Fast NFFT based algorithm for 1d-periodic systems

Similar as in the previous section we derive the fast algorithm now based on Theorem 5.2. The evaluation of the short range part $\phi^{\mathrm{p1,S}}(\boldsymbol{x}_j)$ is done by a direct evaluation again.

5.2.1. Computational approach

Due to Lemma 5.3 we can truncate the infinite sum in $\phi^{\mathrm{p1,L}}(\boldsymbol{x}_j)$, i.e., for some appropriate $M_1 \in 2\mathbb{N}$ we set

$$\phi^{\mathrm{p1,L}}(\boldsymbol{x}_j) \approx \frac{2}{B} \sum_{k \in \mathcal{I}_{M_1} \setminus \{0\}} \sum_{i=1}^{N} q_i \mathrm{e}^{2\pi \mathrm{i} k x_{ij,1}/B} \Theta^{\mathrm{p1}}(k, \|\tilde{\boldsymbol{x}}_{ij}\|).$$

In the following we choose $h > 0$ and $\varepsilon > 0$ such that $\|\tilde{\boldsymbol{x}}_{ij}\| \leq h(1/2 - \varepsilon)$ for all $i, j = 1, \ldots, N$ and define

$$\Theta_0^{\mathrm{p1}}(r) := \gamma + \Gamma(0, \alpha^2 r^2) + \ln(\alpha^2 r^2).$$

In order to approximate the long range part $\phi^{\mathrm{p1,L}}(\boldsymbol{x}_j) + \phi^{\mathrm{p1,0}}(\boldsymbol{x}_j)$ efficiently we consider for $k \in \{0, \ldots, M_1/2\}$ the regularizations

$$K_{\mathrm{R}}(k, r) := \begin{cases} \frac{2}{B}\Theta^{\mathrm{p1}}(k, r) & : k \neq 0, |h^{-1}r| \leq 1/2 - \varepsilon, \\ -\frac{1}{B}\Theta_0^{\mathrm{p1}}(r) & : k = 0, |h^{-1}r| \leq 1/2 - \varepsilon, \\ K_{\mathrm{B}}(k, r) & : |h^{-1}r| \in (1/2 - \varepsilon, 1/2], \\ K_{\mathrm{B}}(k, h/2) & : |h^{-1}r| > 1/2, \end{cases}, \tag{5.7}$$

where each function $K_{\mathrm{B}}(k, \cdot) : [h/2 - h\varepsilon, h/2] \to \mathbb{R}$ is constructed such that $K_{\mathrm{R}}(k, \|\cdot\|) : h\mathbb{T}^2 \to \mathbb{R}$ is in the Sobolev space $\mathcal{H}^p(h\mathbb{T}^2)$, i.e., $K_{\mathrm{B}}(k, \cdot)$ fulfills the interpolation conditions

$$\frac{\partial^j}{\partial r^j} K_{\mathrm{B}}(k, h/2 - h\varepsilon) = \begin{cases} \frac{2}{B}\frac{\partial^j}{\partial r^j}\Theta^{\mathrm{p1}}(k, h/2 - h\varepsilon) & : k \neq 0 \\ -\frac{1}{B}\frac{\mathrm{d}^j}{\mathrm{d}r^j}\Theta_0^{\mathrm{p1}}(h/2 - h\varepsilon) & : k = 0 \end{cases} \quad \text{for } j = 0, \ldots, p-1 \tag{5.8}$$

as well as

$$\frac{\partial^j}{\partial r^j} K_{\mathrm{B}}(k, h/2) = 0 \quad \text{for } j = 1, \ldots, p-1. \tag{5.9}$$

Note that $K_{\mathrm{R}}(k, \|\cdot\|)$ is constant for all the points $\{\boldsymbol{y} \in h\mathbb{T}^2 : \|\boldsymbol{y}\| \geq h/2\}$. Therefore, the conditions (5.9) ensure smoothness of $K_{\mathrm{R}}(k, \|\cdot\|)$ in the points $\{\boldsymbol{y} \in h\mathbb{T}^2 : \|\boldsymbol{y}\| = h/2\}$. Furthermore, (5.9) does not include any restriction on the function value of $K_{\mathrm{R}}(k, h/2)$, since it does not influence the smoothness of $K_{\mathrm{R}}(k, \|\cdot\|)$. In Section 5.2.2 we show that the functions $K_B(k, \|.\|)$ can be constructed as polynomials of degree $2p-2$ by two point Taylor interpolation. By our construction the functions $K_{\mathrm{R}}(k, \|\cdot\|)$ are h-periodic in each direction and smooth, i.e., $K_{\mathrm{R}}(k, \|\cdot\|) \in \mathcal{H}^p(h\mathbb{T}^2)$. For a graphical illustration of a regularization $K_{\mathrm{R}}(k, \cdot)$ see Figure 5.1.

To this end, we approximate for each $k \in \mathcal{I}_{M_1} \setminus \{0\}$ the function

$$\frac{2}{B}\Theta^{\mathrm{p1}}(k, \|\boldsymbol{y}\|) \approx \sum_{\boldsymbol{l} \in \mathcal{I}_{\tilde{\boldsymbol{M}}}} \hat{b}_{k,\boldsymbol{l}} \mathrm{e}^{2\pi \mathrm{i} \boldsymbol{l} \cdot \boldsymbol{y}/h}. \tag{5.10}$$

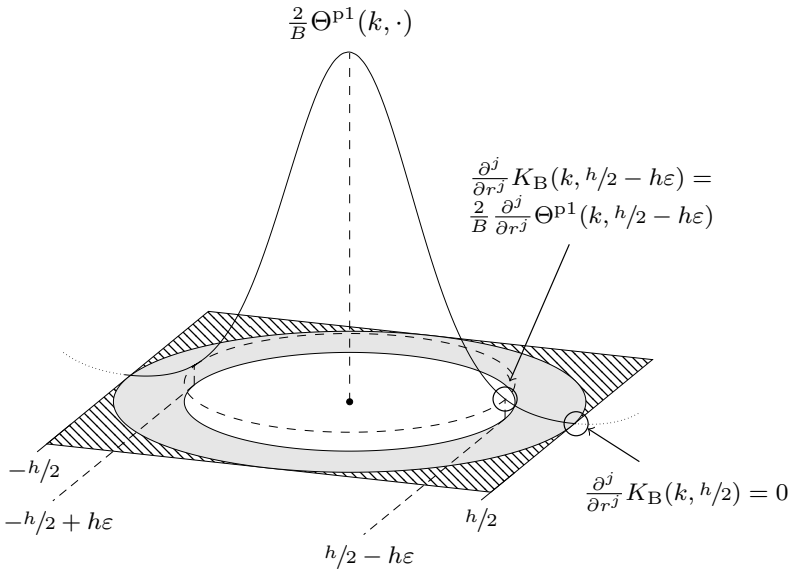

Figure 5.1: Example for $K_{\mathrm{R}}(k,\cdot)$ for $k \geq 1$. Over the gray area the regularization adopts the values of the boundary function $K_{\mathrm{B}}(k,\cdot)$. In the corners (striped area) $K_{\mathrm{R}}(k,\cdot)$ has the constant value $K_{\mathrm{B}}(k,h/2)$. We also marked the points, where the conditions (5.8) and (5.9) are fulfilled.

for $\|\boldsymbol{y}\| \leq h/2 - h\varepsilon$ by a trigonometric polynomial. In the case $k = 0$ we use the approximation

$$-\frac{1}{B}\Theta_0^{\mathrm{p1}}(\alpha^2\|\boldsymbol{y}\|^2) \approx \sum_{\boldsymbol{l}\in\mathcal{I}_{\tilde{\boldsymbol{M}}}} \hat{b}_{0,\boldsymbol{l}}\mathrm{e}^{2\pi\mathrm{i}\boldsymbol{l}\cdot\boldsymbol{y}/h}. \tag{5.11}$$

Thereby, we choose $\tilde{\boldsymbol{M}} = (M_2, M_3) \in 2\mathbb{N}^2$ large enough and compute the Fourier coefficients $\hat{b}_{k,\boldsymbol{l}}$ by

$$\hat{b}_{k,\boldsymbol{l}} := \frac{1}{|\mathcal{I}_{\tilde{\boldsymbol{M}}}|}\sum_{\boldsymbol{j}\in\mathcal{I}_{\tilde{\boldsymbol{M}}}} K_{\mathrm{R}}\left(k, \|\boldsymbol{j}\odot\tilde{\boldsymbol{M}}^{-1}\|h\right)\mathrm{e}^{-2\pi\mathrm{i}\boldsymbol{j}\cdot(\boldsymbol{l}\odot\tilde{\boldsymbol{M}}^{-1})} \tag{5.12}$$

for all $k \in \mathcal{I}_{M_1}$. In summary we obtain the following approximation for the long range parts

$$\begin{aligned}\phi^{\mathrm{p1,L}}(\boldsymbol{x}_j) + \phi^{\mathrm{p1},0}(\boldsymbol{x}_j) &\approx \sum_{k\in\mathcal{I}_{M_1}}\sum_{\boldsymbol{l}\in\mathcal{I}_{\tilde{\boldsymbol{M}}}} \hat{b}_{|k|,\boldsymbol{l}}\sum_{i=1}^{N} q_i\mathrm{e}^{2\pi\mathrm{i}kx_{ij,1}/B}\mathrm{e}^{2\pi\mathrm{i}\boldsymbol{l}\cdot\tilde{\boldsymbol{x}}_{ij}/h}\\ &= \sum_{(k,\boldsymbol{l})\in\mathcal{I}_{\boldsymbol{M}}} \hat{b}_{|k|,\boldsymbol{l}}\left(\sum_{i=1}^{N} q_i\mathrm{e}^{2\pi\mathrm{i}\boldsymbol{v}(k,\boldsymbol{l})\cdot\boldsymbol{x}_i}\right)\mathrm{e}^{-2\pi\mathrm{i}\boldsymbol{v}(k,\boldsymbol{l})\cdot\boldsymbol{x}_j},\end{aligned} \tag{5.13}$$

where we use the truncated Fourier series (5.10), (5.11) in Theorem 5.2 and define $\boldsymbol{M} := (M_1, \tilde{\boldsymbol{M}}) \in 2\mathbb{N}^3$ as well as the vectors $\boldsymbol{v}(k,\boldsymbol{l}) := (k/B, \boldsymbol{l}/h)$.

The expressions in the inner brackets

$$\hat{S}(k,\boldsymbol{l}) := \sum_{i=1}^{N} q_i\mathrm{e}^{2\pi\mathrm{i}\boldsymbol{v}(k,\boldsymbol{l})\cdot\boldsymbol{x}_i}, \quad (k,\boldsymbol{l}) \in \mathcal{I}_{\boldsymbol{M}} \tag{5.14}$$

can be computed by an NFFT$^{\mathrm{H}}$. This will be followed by $|\mathcal{I}_{\boldsymbol{M}}|$ multiplications with $\hat{b}_{|k|,\boldsymbol{l}}$ and completed by an NFFT to compute the outer summation with the complex exponentials. The proposed evaluation of $\phi^{\mathrm{p1,L}}(\boldsymbol{x}_j) + \phi^{\mathrm{p1,0}}(\boldsymbol{x}_j)$ at the points $\boldsymbol{x}_j$, $j = 1, \dots, N$, requires $\mathcal{O}(N + |\mathcal{I}_{\boldsymbol{M}}| \log |\mathcal{I}_{\boldsymbol{M}}|)$ arithmetic operations.

For the calculation of the forces we set $\mathcal{S} := \mathbb{Z} \times \{0\}^2$, define $\boldsymbol{F}^{\mathrm{p1}}(\boldsymbol{x}_j) := \boldsymbol{F}_{\mathcal{S}}(\boldsymbol{x}_j)$ via (1.4) and calculate the short range portions $\boldsymbol{F}^{\mathrm{p1,S}}(\boldsymbol{x}_j)$, as defined in (3.5), by a direct summation. In the long range part we can either use the i$\boldsymbol{k}$ approach, i.e., we set

$$\boldsymbol{F}^{\mathrm{p1,L}}(\boldsymbol{x}_j) + \boldsymbol{F}^{\mathrm{p1,0}}(\boldsymbol{x}_j) \approx 2\pi \mathrm{i} q_j \sum_{(k,\boldsymbol{l}) \in \mathcal{I}_{\boldsymbol{M}}} \hat{b}_{|k|,\boldsymbol{l}} \left(\sum_{i=1}^{N} q_i \mathrm{e}^{2\pi \mathrm{i} \boldsymbol{v}(k,\boldsymbol{l}) \cdot \boldsymbol{x}_i} \right) \boldsymbol{v}(k,\boldsymbol{l}) \mathrm{e}^{-2\pi \mathrm{i} \boldsymbol{v}(k,\boldsymbol{l}) \cdot \boldsymbol{x}_j}, \quad (5.15)$$

or the analytic differentiation, cf. (3.6).

In summary, we obtain Algorithm 4.3 for the fast computation of 1d-periodic Coulomb interactions.

Algorithm 5.5 (1d-periodic P^{2}NFFT)**.**

Input: Positions $\boldsymbol{x}_j \in B\mathbb{T} \times [-B_2/2, B_2/2] \times [-B_3/2, B_3/2]$, charges $q_j \in \mathbb{R}$ $(j = 1, \dots, N)$, splitting parameter $\alpha > 0$, short range cutoff $r_{\mathrm{cut}} > 0$, long range cutoff $\boldsymbol{M} = (M_1, \tilde{\boldsymbol{M}}) \in 2\mathbb{N}^3$, regularization parameter $\varepsilon > 0$, degree of smoothness $p \in \mathbb{N}$.

0.) Precomputations:
   a) Set $h := (1/2 - \varepsilon)^{-1} \sqrt{B_2^2 + B_3^2}$.
   b) Construct the regularization (5.7) for each $k \in \{0, \dots, M_1/2\}$.
   c) Compute the Fourier coefficients (5.12).

1.) Compute the short range parts of the potentials $\phi^{\mathrm{p1,S}}(\boldsymbol{x}_j)$ and the short range parts of the forces $\boldsymbol{F}^{\mathrm{p1,S}}(\boldsymbol{x}_j)$ by direct evaluation, i.e., restrict the summation in (5.5) and (3.5), where $\mathcal{S} := \mathbb{Z} \times \{0\}^2$, to all $\|\boldsymbol{x}_{ij} + B\boldsymbol{n}\| \leq r_{\mathrm{cut}}$.

2.) Compute the sums $\hat{S}(k, \boldsymbol{l})$ in (5.14) by the adjoint NFFT (2.4).

3.) Apply the NFFT (2.2) to compute the long range parts of the potentials $\phi^{\mathrm{p1,L}}(\boldsymbol{x}_j) + \phi^{\mathrm{p1,0}}(\boldsymbol{x}_j)$ by (5.13).

4.) Compute the long range parts of the forces $\boldsymbol{F}^{\mathrm{p1,L}}(\boldsymbol{x}_j) + \boldsymbol{F}^{\mathrm{p1,0}}(\boldsymbol{x}_j)$ via the i$\boldsymbol{k}$ differentiation approach (5.15) or the analytic differentiation, cf. (3.6).

5.) For all $j = 1, \dots, N$ compute

$$\begin{aligned} \phi^{\mathrm{p1}}(\boldsymbol{x}_j) &= \phi^{\mathrm{p1,S}}(\boldsymbol{x}_j) + \phi^{\mathrm{p1,L}}(\boldsymbol{x}_j) + \phi^{\mathrm{p1,0}}(\boldsymbol{x}_j) + \phi^{\mathrm{p1,self}}(\boldsymbol{x}_j) \\ \boldsymbol{F}^{\mathrm{p1}}(\boldsymbol{x}_j) &= \boldsymbol{F}^{\mathrm{p1,S}}(\boldsymbol{x}_j) + \boldsymbol{F}^{\mathrm{p1,L}}(\boldsymbol{x}_j) + \boldsymbol{F}^{\mathrm{p1,0}}(\boldsymbol{x}_j). \end{aligned}$$

6.) Compute the energy (4.2).

Output: Energy U^{p1}, potentials $\phi^{\mathrm{p1}}(\boldsymbol{x}_j)$ and forces $\boldsymbol{F}^{\mathrm{p1}}(\boldsymbol{x}_j)$.

Remark 5.6. Algorithm 5.5 has the same structure as the NFFT based method for 3d-periodic systems, cf. Section 3. Thus, we also obtain a matrix vector notation of the form (3.4) for the approximation of $\phi^{\mathrm{p1,L}}(\boldsymbol{x}_j) + \phi^{\mathrm{p1,0}}(\boldsymbol{x}_j)$. In other words, we use the same algorithm, where we replace the Fourier coefficients $\hat{b}_{\boldsymbol{k}}$ from (3.3) by the new coefficients $\hat{b}_{k,\boldsymbol{l}}$ in (5.12) and insert the nodes $(x_{ij,1}/h, \tilde{\boldsymbol{x}}_{ij}/B) \in \mathbb{T}^3$ instead of $\boldsymbol{x}_{ij}/B \in \mathbb{T}^3$ into the NFFT algorithms. □

5.2.2. Implementation details

The precomputation step of Algorithm 5.5 includes the construction of the regularizations (5.7). Thereby, we obtain $K_{\mathrm{B}}(k,\cdot)$ by the unique polynomial of degree $2p-2$ that fulfills the $2p-1$ interpolation conditions (5.8) – (5.9). An explicit representation of this polynomial is given by Theorem A.2 in the appendix, where we set $m = h(1/2 - \varepsilon/2)$, $r = h\varepsilon/2$ and a_j, b_j equal to the right hand side of the interpolation conditions (5.8) – (5.9), respectively.

In order to compute the derivatives in (5.8) – (5.9) we use the following relations. At first, we consider the function $\Theta^{\mathrm{p1}}(k,r)$ as defined in (5.6) and show that it can be expressed in terms of an incomplete modified Bessel function of the second kind [19] defined by

$$K_\nu(x,y) := \int_1^\infty t^{-\nu-1} \mathrm{e}^{-xt-y/t} \mathrm{d}t, \quad \nu \in \mathbb{R}, x \geq 0, y \geq 0.$$

Indeed, with the substitution $t = \alpha^2/z^2$ in (5.6) we get

$$\Theta^{\mathrm{p1}}(k,r) = \int_0^\alpha \frac{1}{z} \mathrm{e}^{\frac{-\pi^2k^2}{B^2z^2}} \mathrm{e}^{-r^2z^2} \mathrm{d}z \overset{t=\alpha^2/z^2}{=} \frac{1}{2} \int_1^\infty t^{-1} \mathrm{e}^{-\frac{\pi^2k^2}{\alpha^2B^2}t - \alpha^2r^2t^{-1}} \mathrm{d}t = \frac{1}{2} K_0\left(\frac{\pi^2k^2}{\alpha^2B^2}, \alpha^2r^2\right).$$

Note that the relation [19]

$$\frac{\partial K_\nu(x,y)}{\partial y} = -K_{\nu+1}(x,y) \tag{5.16}$$

gives an easy way to compute the necessary partial derivatives. In the following Lemma 5.7 we give a formula for the partial derivatives of $K_0(x,y^2)$ with respect to y, which are needed for the differentiation of the function $\Theta^{\mathrm{p2}}(k,\cdot)$.

Lemma 5.7. *For $x \in \mathbb{R}$ fixed and $k \in \mathbb{N}_0$ we have*

$$\frac{\partial^{2k}}{\partial y^{2k}} K_0(x,y^2) = \sum_{l=0}^{k} \alpha_{k,l} K_{k+l}(x,y^2) y^{2l} \tag{5.17}$$

$$\frac{\partial^{2k+1}}{\partial y^{2k+1}} K_0(x,y^2) = \sum_{l=0}^{k} \beta_{k,l} K_{k+1+l}(x,y^2) y^{2l+1}, \tag{5.18}$$

where the coefficients $\alpha_{k,l}$ and $\beta_{k,l}$ are given recursively by

$$\alpha_{0,0} = 1$$

$$\beta_{k,l} = \begin{cases} -2\alpha_{k,k} & : l = k \\ -2\alpha_{k,l} + 2(l+1)\alpha_{k,l+1} & : \textit{else} \end{cases}$$

$$\alpha_{k,l} = \begin{cases} \beta_{k-1,0} & : k \geq 1, l = 0 \\ -2\beta_{k-1,l-1} & : k \geq 1, l = k \\ -2\beta_{k-1,l-1} + (2l+1)\beta_{k-1,l} & : k \geq 1, \textit{else}. \end{cases}$$

Proof. Induction in k. Via the chain rule and relation (5.16) we have

$$\frac{\partial}{\partial y} K_0(x,y^2) = -2yK_1(x,y^2).$$

Thus, the claim is true for $k = 0$. If (5.18) holds for $k - 1 \geq 0$, we obtain

$$\begin{aligned}\frac{\partial}{\partial y}\left(\frac{\partial^{2k-1}}{\partial y^{2k-1}}K_0(x,y^2)\right) &= \sum_{l=0}^{k-1} -2\beta_{k-1,l}y^{2l+2}K_{k+l+1}(x,y^2) + \sum_{l=0}^{k-1}(2l+1)\beta_{k-1,l}y^{2l}K_{k+l}(x,y^2) \\ &= \sum_{l=1}^{k} -2\beta_{k-1,l-1}y^{2l}K_{k+l}(x,y^2) + \sum_{l=0}^{k-1}(2l+1)\beta_{k-1,l}y^{2l}K_{k+l}(x,y^2),\end{aligned}$$

which shows the choice of the coefficients $\alpha_{k,l}$ in (5.17). For the derivative of order $2k+1$ we get

$$\begin{aligned}\frac{\partial}{\partial y}\left(\frac{\partial^{2k}}{\partial y^{2k}}K_0(x,y^2)\right) &= \sum_{l=0}^{k} -2\alpha_{k,l}y^{2l+1}K_{k+l+1}(x,y^2) + \sum_{l=1}^{k} 2l\alpha_{k,l}y^{2l-1}K_{k+l}(x,y^2) \\ &= \sum_{l=0}^{k} -2\alpha_{k,l}y^{2l+1}K_{k+l+1}(x,y^2) + \sum_{l=0}^{k-1} 2(l+1)\alpha_{k,l+1}y^{2l+1}K_{k+l+1}(x,y^2),\end{aligned}$$

which completes the proof. ■

We implemented the iterative algorithm given in [36] for the computation of the incomplete modified Bessel function of the second kind $K_\nu(x,y)$ for arbitrary order $\nu \in \mathbb{R}$. In our algorithm, we evaluate this function with an absolute accuracy of $\epsilon = 10^{-15}$. However, this iteration gets numerical problems for large values of x and y because the very small numbers due to the exponential damping within the integral. Therefore, we compute the following upper bounds on $K_\nu(x,y)$ and assume $K_\nu(x,y)$ to be numerically equal to zero whenever one of these bounds is already very small. For $\nu \geq -1$ an upper bound is given by

$$K_\nu(x,y) \leq \int_1^\infty \frac{\mathrm{e}^{-xt}}{t^{\nu+1}}\mathrm{d}t \leq \int_1^\infty \mathrm{e}^{-xt}\mathrm{d}t = \frac{\mathrm{e}^{-x}}{x}. \tag{5.19}$$

For $K_0(x,\cdot)$ and its derivatives we always have $\nu \geq 0$, cf. (5.16). However, for $x < y$ it was suggested [36] to evaluate the faster convergent complement integral

$$K_\nu(x,y) = 2(x/y)^{\nu/2}K_\nu(2\sqrt{xy}) - K_{-\nu}(y,x), \tag{5.20}$$

where the Bessel function $K_\nu(\cdot)$ is defined by

$$K_\nu(z) := \frac{1}{2}\int_0^\infty \frac{\mathrm{e}^{-z/2(t+1/t)}}{t^{\nu+1}}\mathrm{d}t,$$

cf. [19]. Thus, we also have to consider the case $\nu < -1$. Here, we set $n := -\nu - 1 \geq 1$ and obtain the upper bounds

$$\begin{aligned}K_\nu(x,y) &\leq \int_1^\infty \frac{\mathrm{e}^{-xt}}{t^{\nu+1}}\mathrm{d}t = \int_1^\infty t^n\mathrm{e}^{-xt}\mathrm{d}t = \mathrm{e}^{-x}\sum_{k=0}^{n}\frac{n!}{(n-k)!}\frac{1}{x^{k+1}} \\ &\leq \begin{cases} \dfrac{\mathrm{e}^{-x}n!}{x^{n+1}}\displaystyle\sum_{k=0}^{n}\frac{1}{(n-k)!} \leq \frac{\mathrm{e}^{1-x}n!}{x^{n+1}} & : x \leq 1 \\ \dfrac{\mathrm{e}^{-x}n!}{x}\displaystyle\sum_{k=0}^{n}\frac{1}{(n-k)!} \leq \frac{\mathrm{e}^{1-x}n!}{x} & : x > 1 \end{cases}.\end{aligned}$$

By (5.20) we obtain another upper bound for $K_\nu(x,y)$ in the case $\nu \geq -1$, namely,

$$K_\nu(x,y) < 2(x/y)^{\nu/2} K_\nu(2\sqrt{xy}) \leq (x/y)^{\nu/2} \int_0^\infty \mathrm{e}^{-t\sqrt{xy}/2} \mathrm{d}t = 2(x/y)^{\nu/2} \frac{\mathrm{e}^{-\sqrt{xy}/2}}{\sqrt{xy}}.$$

This gives often a better estimate than (5.19) especially if $x < y$.

Another numerical difficulty appears in (5.12) for $k \neq 0$ when K_R must be evaluated near the origin. This corresponds to the evaluation of $K_0(x,y)$ with small x and y, where the evaluation of the function is numerically demanding and the accuracy ϵ can not always be achieved. However, we have

$$\left.\frac{\partial^n K_0(x,y)}{\partial y^n}\right|_{y=0} = (-1)^n K_n(x,0) = (-1)^n x^n \int_x^\infty \mathrm{e}^{-t} t^{-n-1} \mathrm{d}t = (-1)^n x^n \Gamma(-n,x) \tag{5.21}$$

with the upper incomplete gamma function Γ, as defined in (5.2). Therewith, we obtain for fixed x and $m \in \mathbb{N}$

$$K_0(x,y) = \sum_{n=0}^{m} \frac{(-1)^n}{n!} x^n \Gamma(-n,x) y^n + R_m K_0(x,0)$$

where for some $0 < \xi < 1$

$$R_m K_0(x,0) = \frac{(-1)^{m+1} K_{m+1}(x,\xi y)}{(m+1)!} y^{m+1}.$$

Applying (5.19) we compute the upper bound

$$|R_m K_0(x,0)| \leq \frac{K_{m+1}(x,0) y^{m+1}}{(m+1)!} \leq \frac{\mathrm{e}^{-x} y^{m+1}}{(m+1)! x}.$$

Thus, for x and y small we calculate the value of the truncated Taylor series in (5.21), where we choose m large enough to fulfill $|R_m K_0(x,0)| < \epsilon$.

In order to compute the Fourier coefficients $\hat{b}_{0,l}$, we also have to evaluate the functions $\Gamma(0,\alpha^2 r^2)$ and $\ln(\alpha^2 r^2)$ as well as their derivatives. In the following Lemma we show how the derivatives of $\Gamma(0,x^2)$ can be computed recursively.

Lemma 5.8. *For $k \in \mathbb{N}$ we have*

$$\frac{\mathrm{d}^{2k}}{\mathrm{d}x^{2k}} \Gamma(0,x^2) = 2\mathrm{e}^{-x^2} \left(\sum_{l=1}^{k} \frac{(2k-1)!}{(k-l)!} x^{-2l} + p_k(x) \right) \tag{5.22}$$

$$\frac{\mathrm{d}^{2k+1}}{\mathrm{d}x^{2k+1}} \Gamma(0,x^2) = -2\mathrm{e}^{-x^2} \left(\sum_{l=0}^{k} \frac{(2k)!}{(k-l)!} x^{-(2l+1)} + q_k(x) \right) \tag{5.23}$$

where p_k and q_k are polynomials of degree $2k-2$ and $2k-1$, respectively, fulfilling the recursion

$$\begin{aligned} p_1(x) &= 2 \\ q_k(x) &= 2x p_k(x) - \frac{\mathrm{d}}{\mathrm{d}x} p_k(x) \\ p_{k+1}(x) &= 2x q_k(x) - \frac{\mathrm{d}}{\mathrm{d}x} q_k(x) + \frac{2(2k)!}{k!}. \end{aligned}$$

Proof. Induction in $k \in \mathbb{N}$. We have

$$\frac{\mathrm{d}^2}{\mathrm{d}x^2}\Gamma(0,x^2) = \frac{\mathrm{d}}{\mathrm{d}x}\left(\frac{-2\mathrm{e}^{-x^2}}{x}\right) = 2\mathrm{e}^{-x^2}\left(\frac{1}{x^2}+2\right),$$

which shows the validity of (5.22) for $k=1$ with $p_1(x)=2$. If (5.22) holds for some $k \in \mathbb{N}$ we have

$$\begin{aligned}\tfrac{\mathrm{d}}{\mathrm{d}x}\tfrac{\mathrm{d}^{2k}}{\mathrm{d}x^{2k}}\Gamma(0,x^2) =& -4x\mathrm{e}^{-x^2}\left(\sum_{l=1}^{k}\tfrac{(2k-1)!}{(k-l)!}x^{-2l}+p_k(x)\right)\\ &+2\mathrm{e}^{-x^2}\left(-\sum_{l=1}^{k}\tfrac{2l(2k-1)!}{(k-l)!}x^{-(2l+1)}+\tfrac{\mathrm{d}}{\mathrm{d}x}p_k(x)\right).\end{aligned}$$

If we define the polynomial q_k of degree $2k-1$ as $q_k(x) := 2xp_k(x) - \frac{\mathrm{d}}{\mathrm{d}x}p_k(x)$ we obtain

$$\begin{aligned}\tfrac{\mathrm{d}^{2k+1}}{\mathrm{d}x^{2k+1}}\Gamma(0,x^2) &= -2\mathrm{e}^{-x^2}\left(\sum_{l=0}^{k-1}\tfrac{2(2k-1)!}{(k-l-1)!}x^{-(2l+1)}+\sum_{l=1}^{k}\tfrac{2l(2k-1)!}{(k-l)!}x^{-(2l+1)}+q_k(x)\right)\\ &= -2\mathrm{e}^{-x^2}\left(\tfrac{(2k)!}{k!}x^{-1}+\sum_{l=1}^{k-1}\tfrac{(2k-1)![2(k-l)+2l]}{(k-l)!}x^{-(2l+1)}+\tfrac{(2k)!}{0!}x^{-(2k+1)}+q_k(x)\right),\end{aligned}$$

which is equivalent to (5.23). For the derivatives of order $2k+2$ we get

$$\begin{aligned}\tfrac{\mathrm{d}}{\mathrm{d}x}\tfrac{\mathrm{d}^{2k+1}}{\mathrm{d}x^{2k+1}}\Gamma(0,x^2) =& 4x\mathrm{e}^{-x^2}\left(\sum_{l=0}^{k}\tfrac{(2k)!}{(k-l)!}x^{-(2l+1)}+q_k(x)\right)\\ &+2\mathrm{e}^{-x^2}\left(\sum_{l=0}^{k}\tfrac{(2l+1)(2k)!}{(k-l)!}x^{-(2l+2)}-\tfrac{\mathrm{d}}{\mathrm{d}x}q_k(x)\right).\end{aligned}$$

Setting $p_{k+1}(x) := 2xq_k(x) + \frac{2(2k)!}{k!} - \frac{\mathrm{d}}{\mathrm{d}x}q_k(x)$ we obtain

$$\begin{aligned}\tfrac{\mathrm{d}^{2k+2}}{\mathrm{d}x^{2k+2}}\Gamma(0,x^2) &= 2\mathrm{e}^{-x^2}\left(\sum_{l=1}^{k}\tfrac{2(2k)!}{(k-l)!}x^{-2l}+\sum_{l=1}^{k+1}\tfrac{(2l-1)(2k)!}{(k-l+1)!}x^{-2l}+p_{k+1}(x)\right)\\ &= 2\mathrm{e}^{-x^2}\left(\sum_{l=1}^{k}\tfrac{(2k)![2(k-l+1)+2l-1]}{(k-l+1)!}x^{-2l}+\tfrac{(2k+1)(2k)!}{0!}x^{-2(k+1)}+p_{k+1}(x)\right).\end{aligned}$$

■

5.3. Numerical Results

In this section we present numerical results of our algorithm for 1d-periodic systems. We set up the tests analogously to the 2d-periodic case, see Section 4.3 for details.

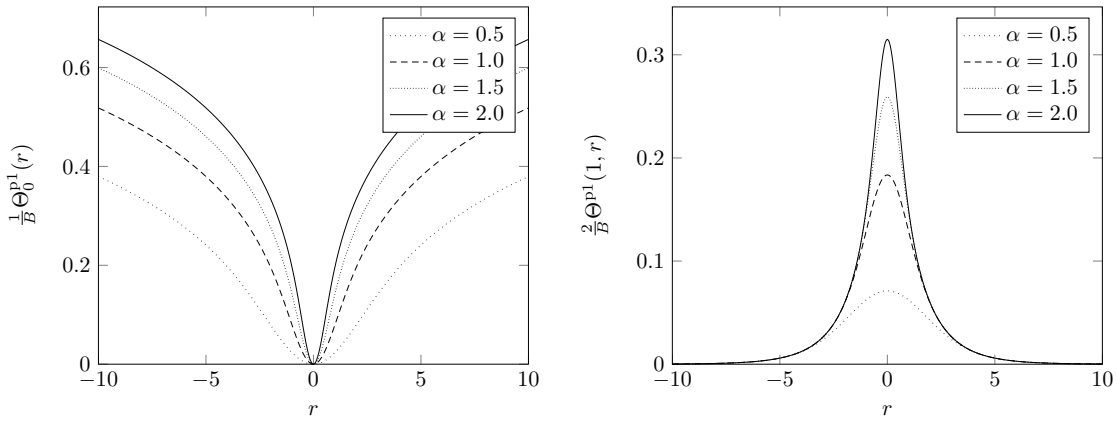

Figure 5.2: $\Theta_0^{\mathrm{p1}}(r)$ and $\Theta^{\mathrm{p1}}(1,r)$ with $B = 10$ for different splitting parameters α.

Example 5.9. As in Example 4.5 we consider the cloud wall system with $N = 300$ charged particles and compute the potentials as well as the forces subject to 1d-periodic boundary conditions. Again, we plot the functions $\Theta^{\mathrm{p1}}(1,\cdot)$ as well as $\Theta_0^{\mathrm{p1}}(\cdot)$ over the interval $[-B, B]$ for different splitting parameters α, see Figure 5.2.

We tested Algorithm 5.5 with the smoothness $p = 6$, the short range cutoff $r_{\mathrm{cut}} = 4$ and $\boldsymbol{M} = (64, 64, 64)$. Within the NFFT computations we chose $\boldsymbol{m} = (64, 128, 128)$ in (2.3) and the cardinal B-Spline of order 8 as a window function.

In Figure 5.3 we plot the rms field errors $\triangle E_{\mathbb{Z}\times\{0\}^2}$ with respect to the splitting parameter α for different values of ε. We observe similar patterns as in the case for 2d-periodic boundary conditions. We see that we obtain a considerably different optimal value for ε. We obtain the smallest error for $\varepsilon \approx 0.115$, where $\alpha \approx 0.9$ is optimal.

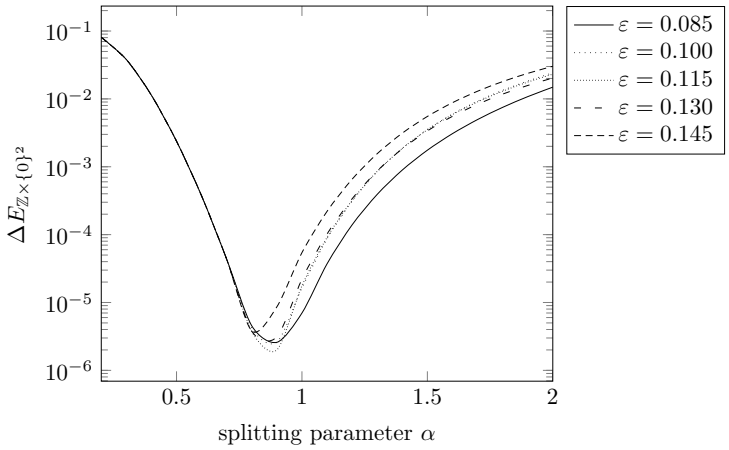

Figure 5.3: Relative rms field error (1.7) over α for different regularization parameters ε. We choose the short range cutoff $r_{\mathrm{cut}} = 4$, $p = 6$, $\boldsymbol{M} = (64, 64, 64)$, $\boldsymbol{m} = (64, 128, 128)$ and the B-Spline of order 8 as NFFT window function φ in Algorithm 5.5.

In Figure 5.4 we plot the rms field error $\triangle E_{\mathbb{Z}\times\{0\}^2}$ with respect to the splitting parameter α for different long range cutoffs $\boldsymbol{M} = (M, M, M) \in 2\mathbb{N}^3$. Again, the regularization parameter ε is tuned by hand to obtain a small optimal rms field error. On the right hand side we see the

corresponding errors produced by the 3d-periodic computation. As in the case for 2d-periodic boundary conditions we obtain smaller errors in the 3d-periodic case, which implies that also the optimal values for the splitting parameter α differ. □

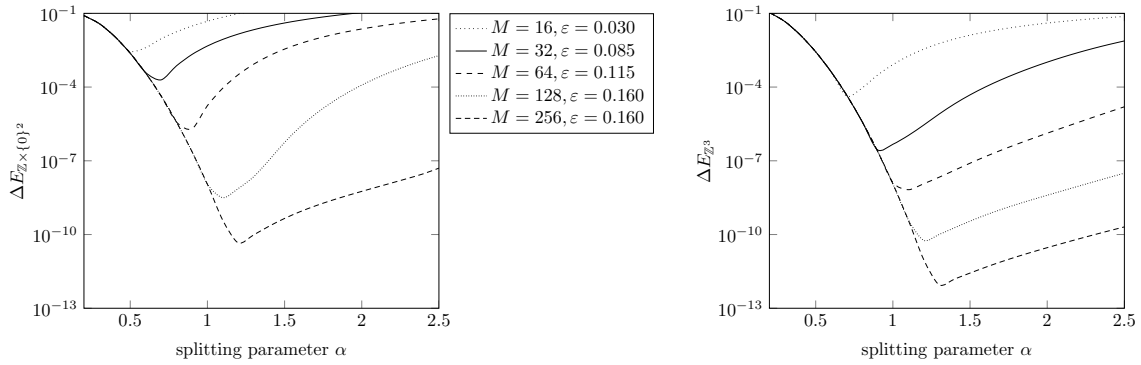

Figure 5.4: The relative rms field error (1.7) over α for different FFT sizes. We choose the short range cutoff $r_{\text{cut}} = 4$, $p = 6$, $\boldsymbol{m} = (M, 2M, 2M)$ and the B-Spline of order 8 as NFFT window function φ in Algorithm 5.5. We plot the results of the 1d-periodic (left) as well as of the 3d-periodic computation (right).

Example 5.10. We apply our Algorithm to the particle systems we already considered in Example 4.6. We set $r_{\text{cut}} = 4$ and compute the potentials as well as the forces in the system with $N = 300$ particles with the far field cutoff $\boldsymbol{M} = (M, M, M) = (16, 16, 16)$. We found that the rms field error $\triangle E_{\mathbb{Z}\times\{0\}^2}$ is minimized for the splitting parameter $\alpha \approx 0.5$ and $\varepsilon \approx 0.03$, see Example 5.9.

As the particle systems have the same particle density we keep the short range cutoff $r_{\text{cut}} = 4$ and the splitting parameter $\alpha = 0.5$ fixed, increase the value of M and vary ε. In order to determine a good choice for ε we proceed as in Example 4.6 and investigate the exactness of our two dimensional approximation (5.11) with respect to M and ε, see Figure 5.5. In the case $M = 16$ we find the optimal value $\varepsilon_{\text{opt}} \approx 0.095$, whereas the relative rms field error error $\triangle E_{\mathbb{Z}\times\{0\}^2}$ is minimized for $\varepsilon \approx 0.03 \approx 0.3158 \cdot 0.095$. Thus, we heuristically choose $\varepsilon = 0.3158 \cdot \varepsilon_{\text{opt}}$ in our computations. Obviously, the error is not that much dominated by the error in the $k = 0$ part as in the 2d-periodic case. The obtained errors can be found in Table 5.1. Again, we computed the errors produced by Algorithm 5.5 without as well as with oversampling, where $\boldsymbol{m} = (M, 2M, 2M)$. In Figure 5.6 we plot the corresponding run times. □

6. Conclusion

In this paper we proposed new fast algorithms for the computation of the potentials and the forces in three-dimensional particle systems subject to 2d- and 1d-periodic boundary conditions. These algorithms are based on the Ewald summation formulas, which we combined with the NFFT based fast summation method. Therefore, we obtain the same structure as the well known NFFT based methods for open as well as for fully periodic boundary conditions.

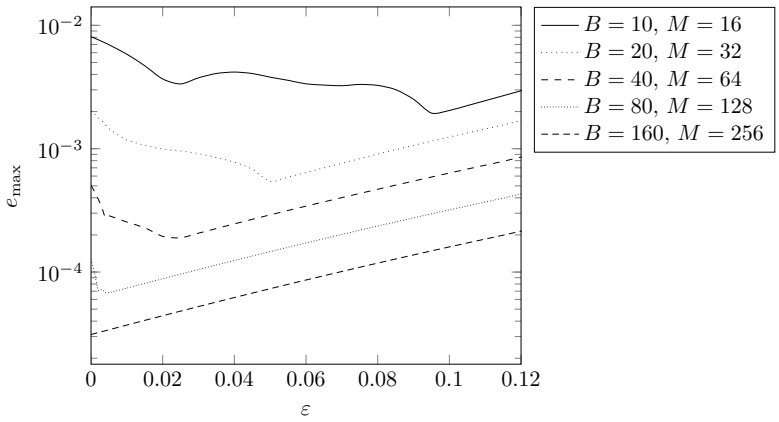

Figure 5.5: Maximum approximation error (5.11) for $k = 0$ over ε, where we choose $\alpha = 0.5$.

				oversampling	no oversampling	
N	B	ε	M	$\Delta E_{\mathbb{Z}\times\{0\}^2}$	$\Delta E_{\mathbb{Z}\times\{0\}^2}$	$\Delta E_{\mathbb{Z}^3}$
300	10	3.0000e-02	16	2.8812e-03	4.9664e-03	2.7126e-03
2400	20	1.5789e-02	32	2.9800e-03	4.1694e-03	2.7126e-03
19200	40	7.8947e-03	64	3.2359e-03	3.6469e-03	2.7126e-03
153600	80	1.5789e-03	128	3.2345e-03	3.6396e-03	2.7126e-03
1228800	160	3.1579e-05	256	3.2837e-03	3.6283e-03	2.7126e-03

Table 5.1: Relative rms force errors in the cloud wall systems under 1d-periodic boundary conditions (with and without oversampling in the last two dimensions) as well as under fully periodic boundary conditions. These errors have been obtained with the short range cutoff $r_{\text{cut}} = 4$ and the splitting parameter $\alpha = 0.5$.

In addition to the splitting parameter α, the near field, and the far field cutoffs, the proposed algorithms require numerous other parameters as input. On the one hand, we need to set the NFFT specific parameters, as the type of the window function φ and related cutoffs, and, on the other hand, we have to specify the degree of smoothness p as well as the regularization parameter ε, which are needed for the fast summation.

Of course, without exact error estimates the task of tuning all parameters optimally is demanding. In our numerical examples we especially concentrated on the choice of the splitting parameter α and the regularization parameter ε in dependance on the far field cutoff $\boldsymbol{M}$. We plotted the behavior of the relative rms field error over α for different $\boldsymbol{M}$, where the parameter ε was tuned by hand. In summary, we have to point out that the overall error very much depends on the choice of ε, which seems to adopt different optimal values in the 2d- and the 1d-periodic case. Furthermore, in comparison with the fully periodic case we have seen that the algorithms for mixed periodic boundary conditions produce slightly larger errors in the long range part. Thus, also the choice of the splitting parameter α has to be adjusted.

In contrast to the fully periodic case, the Fourier coefficients for the computation of the long range part are computed via the FFT based on sampling the regularized kernel functions. Of course, this produces additional errors and leads to a precomputation step, which has to be done only once if the data are needed repeatedly. Especially the evaluation of the incomplete modified Bessel function in the 1d-periodic case is numerically demanding.

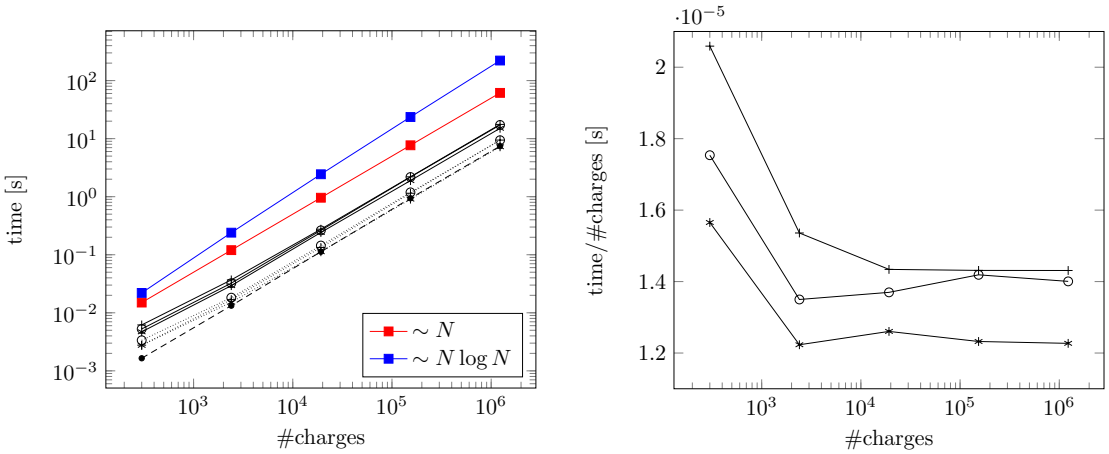

Figure 5.6: Computation times with oversampling (o) and without oversampling (∗) for the 1d-periodic case as well as for the fully periodic computation (+).
left: Attended times for the total computation (solid lines), the long range part (dotted) as well as the short range part (dashed). We also plot exemplary behaviors where the run time grows proportional to N (red) and $N \log N$ (blue).
right: Total computation time scaled by the number of particles.
We achieved rms field errors of the size $\approx 10^{-3}$.

For growing numbers of particles N our algorithms show the same behavior in computational costs as the method for 3d-periodic boundary conditions. Thereby, we were able to keep the relative rms field error almost constant, where the parameter ε was set heuristically.

All in all, the proposed methods compete with the algorithm for 3d-periodic boundary conditions. The deficiency of exactness is inevitable and of a reasonable size. A further objective might be to derive error estimates, similar to the P^3M [14], which allow an automatic tuning of the involved parameters.

Appendix

A. Two point Taylor interpolation

Theorem A.1. *Let an interval $[m-r, m+r], r > 0$, and the interpolation values $a_j = K^{(j)}(m-r)$, $b_j = K^{(j)}(m+r)$, $j = 0, \dots, p-1$, be given. For $y = \frac{x-m}{r}$ the polynomial*

$$\begin{aligned} P(x) &= \sum_{j=0}^{p-1} \sum_{k=0}^{p-1-j} \binom{p-1+k}{k} \frac{1}{j! 2^p 2^k} \left[r^j (1-y)^p (1+y)^{k+j} a_j + (-r)^j (1+y)^p (1-y)^{k+j} b_j \right] \\ &= \sum_{j=0}^{p-1} B(p,j,y) r^j a_j + \sum_{j=0}^{p-1} B(p,j,-y)(-r)^j b_j \end{aligned}$$

of degree $2p-1$ satisfies the interpolation conditions $P^{(j)}(m-r) = a_j, P^{(j)}(m+r) = b_j$, $j = 0, \dots, p-1$. Hereby, the basis polynomials $B(p,j,y)$ are given by

$$B(p,j,y) := \sum_{k=0}^{p-1-j} \binom{p-1+k}{k} \frac{1}{j!2^p 2^k} (1-y)^p (1+y)^{k+j}.$$

Proof. See [3, Corollary 2.2.6] or [17, Proposition 3.2]. ∎

Theorem A.2. *Let an interval $[m-r, m+r], r > 0$, and the interpolation values $a_j = K^{(j)}(m-r)$, $j = 0, \dots, p-1$, and $b_j = K^{(j)}(m+r)$, $j = 1, \dots, p-1$, be given. For $y = \frac{x-m}{r}$ the polynomial*

$$\begin{aligned} Q(x) :=& \sum_{j=0}^{p-2} I(p-1,j,y) r^{j+1} a_{j+1} + \sum_{j=0}^{p-2} I(p-1,j,-y)(-r)^{j+1} b_{j+1} \\ & - \sum_{j=0}^{p-2} I(p-1,j,-1) r^{j+1} a_{j+1} - \sum_{j=0}^{p-2} I(p-1,j,1)(-r)^{j+1} b_{j+1} + a_0 \end{aligned}$$

of degree $2p-2$ satisfies the interpolation conditions $Q^{(j)}(m-r) = a_j, j = 0, \dots, p-1$, and $Q^{(j)}(m+r) = b_j$, $j = 1, \dots, p-1$. Thereby, the polynomials $I(p,j,y)$ are given by

$$I(p,j,y) := \sum_{k=0}^{p-1-j} \binom{p-1+k}{k} \frac{1}{j!2^p 2^k} \sum_{l=0}^{p} \frac{p!}{(p-l)!} \frac{(k+j)!}{(k+1+j+l)!} (1-y)^{p-l} (1+y)^{k+j+1+l}.$$

Proof. According to Theorem A.1 the polynomial

$$\tilde{P}(x) = \sum_{j=0}^{p-2} B(p-1,j,y) r^j a_{j+1} + \sum_{j=0}^{p-2} B(p-1,j,-y)(-r)^j b_{j+1}$$

satisfies the interpolation conditions $\tilde{P}^{(j)}(m-r) = a_{j+1}, \tilde{P}^{(j)}(m+r) = b_{j+1}$, $j = 0, \dots, p-2$. For $k, l \in \mathbb{N}$ we obtain by partial integration for l times

$$\int (1-x)^l (1+x)^k \mathrm{d}x = \sum_{j=0}^{l} \frac{l!}{(l-j)!} \frac{k!}{(k+1+j)!} (1-x)^{l-j} (1+x)^{k+1+j} + C, C \in \mathbb{R}$$

and therewith

$$\int B(p,j,y) \mathrm{d}x = r I(p,j,y) + C, C \in \mathbb{R}.$$

Thus, the antiderivatives of $\tilde{P}(x)$ are given by $Q(x) := \tilde{Q}(x) + C$, $C \in \mathbb{R}$ with

$$\tilde{Q}(x) := \sum_{j=0}^{p-2} I(p-1,j,y) r^{j+1} a_{j+1} + \sum_{j=0}^{p-2} I(p-1,j,-y)(-r)^{j+1} b_{j+1}.$$

Finally, we choose the constant $C = a_0 - \tilde{Q}(m-r)$ in order to satisfy $Q(m-r) = a_0$. ∎

References

[1] *ScaFaCoS - Scalable Fast Coloumb Solvers.* http://www.scafacos.de.

[2] M. Abramowitz and I.A. Stegun (eds.): *Handbook of Mathematical Functions.* National Bureau of Standards, Washington, DC, USA, 1972.

[3] R.P. Agarwal and P.J.Y. Wong: *Error inequalities in polynomial interpolation and their applications*, vol. 262 of *Mathematics and its Applications.* Kluwer Academic Publishers Group, Dordrecht, 1993.

[4] A. Arnold: *Berechnung der elektrostatischen Wechselwirkung in 2d+h periodischen Systemen.* Diplomarbeit, Johannes Gutenberg-Universität, Mainz, 2001.

[5] A. Arnold, M. Bolten, H.D.F. Fahrenberger, F. Gähler, R. Halver, F. Heber, M. Hofmann, J. Iseringhausen, I. Kabadshow, O. Lenz, M. Pippig, D. Potts, and G. Sutmann: *A comparison of scalable fast methods for long-range interactions.* Phys. Rev. E, accepted, 2013.

[6] A. Arnold and C. Holm: *MMM2D: A fast and accurate summation method for electrostatic interactions in 2D slab geometries.* Comput. Phys. Commun., 148:327 – 348, 2002.

[7] A. Arnold and C. Holm: *MMM1D: A method for calculating electrostatic interactions in one-dimensional periodic geometries.* J. Chem. Phys., 123:144103, 2005.

[8] A. Arnold, J. de Joannis, and C. Holm: *Electrostatics in periodic slab geometries. I.* J. Chem. Phys., 117:2496, 2002.

[9] A. Bródka: *Ewald summation method with electrostatic layer correction for interactions of point dipoles in slab geometry.* Chem. Phys. Lett., 400:62 – 67, 2004.

[10] A. Bródka and P. Sliwinski: *Three-dimensional ewald method with correction term for a system periodic in one direction.* J. Chem. Phys., 120:5518 – 5523, 2004.

[11] H. Dachsel: *An error-controlled Fast Multipole Method.* J. Chem. Phys., 132(11):119901, 2010.

[12] T. Darden, D. York, and L. Pedersen: *Particle mesh Ewald: An $N\log(N)$ method for Ewald sums in large systems.* J. Chem. Phys., 98:10089, 1993.

[13] M. Deserno and C. Holm: *How to mesh up Ewald sums. I. A theoretical and numerical comparison of various particle mesh routines.* J. Chem. Phys., 109:7678 – 7693, 1998.

[14] M. Deserno and C. Holm: *How to mesh up Ewald sums. II. An accurate error estimate for the Particle-Particle-Particle-Mesh algorithm.* J. Chem. Phys., 109:7694 – 7701, 1998.

[15] U. Essmann, L. Perera, M.L. Berkowitz, T. Darden, H. Lee, and L.G. Pedersen: *A smooth particle mesh Ewald method.* J. Chem. Phys., 103:8577 – 8593, 1995.

[16] P.P. Ewald: *Die Berechnung optischer und elektrostatischer Gitterpotentiale.* Ann. Phys., 369:253–287, 1921.

[17] M. Fenn and G. Steidl: *Fast NFFT based summation of radial functions.* Sampl. Theory Signal Image Process., 3:1 – 28, 2004.

[18] A. Grzybowski, E. Gwóźdź, and A. Bródka: *Ewald summation of electrostatic interactions in molecular dynamics of a three-dimensional system with periodicity in two directions.* Phys. Rev. B, 61:6706–6712, 2000.

[19] F.E. Harris: *Incomplete Bessel, generalized incomplete gamma, or leaky aquifer functions.* J. Comput. Appl. Math., 215:260 – 269, 2008.

[20] R.W. Hockney and J.W. Eastwood: *Computer simulation using particles.* Taylor & Francis, Inc., Bristol, PA, USA, 1988.

[21] P.H. Hünenberger: *Lattice-sum methods for computing electrostatic interactions in molecular simulations.* In *Simulation and theory of electrostatic interactions in solution*, vol. 17, pp. 17–83. ASCE, 1999.

[22] I. Kabadshow: *Periodic Boundary Conditions and the Error-Controlled Fast Multipole Method.* PhD thesis, Bergische Universität Wuppertal, Jülich, 2012.

[23] I. Kabadshow and H. Dachsel: *The Error-Controlled Fast Multipole Method for Open and Periodic Boundary Conditions.* In G. Sutmann, P. Gibbon, and T. Lippert (eds.): *Fast Methods for Long-Range Interactions in Complex Systems*, IAS-Series, pp. 85 – 113, Jülich, 2011. Forschungszentrum Jülich.

[24] J. Keiner, S. Kunis, and D. Potts: *Using NFFT3 - a software library for various nonequispaced fast Fourier transforms.* ACM Trans. Math. Software, 36:Article 19, 1 – 30, 2009.

[25] S.W. de Leeuw, J.W. Perram, and E.R. Smith: *Simulation of electrostatic systems in periodic boundary conditions. I. Lattice sums and dielectric constants.* Proc. Roy. Soc. London Ser. A, 373:27 – 56, 1980.

[26] D. Lindbo and A.K. Tornberg: *Spectral accuracy in fast Ewald-based methods for particle simulations.* J. Comput. Phys., 230:8744 – 8761, 2011.

[27] D. Lindbo and A.K. Tornberg: *Fast and spectrally accurate Ewald summation for 2-periodic electrostatic systems.* J. Chem. Phys., 136:164111, 2012.

[28] F. Nestler: *Approximationsverfahren zur schnellen Energieberechnung in Partikelsystemen.* Diplomarbeit, Fakultät für Mathematik, Technische Universität Chemnitz, 2012.

[29] F. Nestler and D. Potts: *Fast Ewald summation under 2d- and 1d-periodic boundary conditions based on NFFTs.* Proceedings of the 10th International Conference on Sampling Theory and Applications, 2013.

[30] M. Pippig and D. Potts: *Particle simulation based on nonequispaced fast Fourier transforms.* In G. Sutmann, P. Gibbon, and T. Lippert (eds.): *Fast Methods for Long-Range Interactions in Complex Systems*, IAS-Series, pp. 131 – 158, Jülich, 2011. Forschungszentrum Jülich.

[31] M. Pippig and D. Potts: *Parallel three-dimensional nonequispaced fast Fourier transforms and their application to particle simulation.* SIAM J. Sci. Comput., 35:C411 – C437, 2013.

[32] M. Porto: *Ewald summation of electrostatic interactions of systems with finite extent in two of three dimensions.* J. Phys. A, 33:6211 – 6218, 2000.

[33] D. Potts and G. Steidl: *Fast summation at nonequispaced knots by NFFTs.* SIAM J. Sci. Comput., 24:2013 – 2037, 2003.

[34] D. Potts, G. Steidl, and A. Nieslony: *Fast convolution with radial kernels at nonequispaced knots.* Numer. Math., 98:329 – 351, 2004.

[35] D. Potts, G. Steidl, and M. Tasche: *Fast Fourier transforms for nonequispaced data: A tutorial.* In J.J. Benedetto and P.J.S.G. Ferreira (eds.): *Modern Sampling Theory: Mathematics and Applications*, pp. 247 – 270, Boston, MA, USA, 2001. Birkhäuser.

[36] R.M. Slevinsky and H. Safouhi: *A recursive algorithm for the G transformation and accurate computation of incomplete Bessel functions.* Appl. Numer. Math., 60:1411 – 1417, 2010.

[37] I.C. Yeh and M.L. Berkowitz: *Ewald summation for systems with slab geometry.* J. Chem. Phys., 111:3155 – 3162, 1999.